University of South-Eastern Norway

www.usn.no

FMH606 Master's Thesis 2023

Energy and Environmental Technology

Comparing wind farm production data to engineering wake model simulations

Mersal Al Halabi

Faculty of Technology, Natural sciences, and Maritime Sciences

Campus Porsgrunn

University of South-Eastern Norway

www.usn.no

Course: FMH606 Master's Thesis, 2023

Title: Comparing wind farm production data to engineering wake model simulations

A number of pages: 64

Keywords: Pywake, HornsRev1, Power deficit, Normalized power, NOJ, BastankhahGaussian, TurbOPark.

Student: Mersal Al Halabi

Supervisor: Geir Elseth, Equinor Porsgrunn

External partner: Atle Johnsen Gyllensteen, Equinor Porsgrunn

Summary:

With the growing global demand for offshore wind energy, it is imperative to design wind farms in an optimal and efficient manner. However, a challenge arises when wind turbines are grouped together, as wake interactions between them can cause downstream wind speeds to decrease, leading to a reduction in power production. Several wake models are available to simulate this effect and aid engineers in optimizing wind farm designs.

This thesis report compare several offshore wind farms and evaluates the accuracy of commonly used wake models for assessing wake losses in offshore wind farms. The aim is to provide insight into the accuracy of these models in estimating power output while taking wake effects into account. Three wake models: NOJ, BastankhahGaussian, and TurbOPark, implemented in the Pywake tool, were compared using data collected from previous studies on Horns Rev 1 offshore wind farm as a reference. While all models showed some errors in estimating real power production, the TurbOPark model gave the closest result to the real Annual Energy Production value and was able to predict the pattern of power variation while overestimating it. The NOJ provided good agreement with observed data in estimating the power deficit of the entire farm, while all models produced similar results for the normalized power of turbines in row 7. These findings suggest that the Pywake wake models can be considered reliable tools for optimizing offshore wind farm production.

Preface

I am delighted to have pursued my academic journey in the Energy and Environmental Technology master's program at the University of South-Eastern Norway, campus Porsgrunn, which provides a truly global learning environment. It is a dream that came true for me.

This thesis, presented for the completion of my master's degree in Energy and Environmental Technology, carries 30 credits. A description of the thesis is available in appendix A.

I would like to express my heartfelt gratitude to my thesis supervisor, Geir Elseth, and his colleague Atle Johnsen Gyllensteen, from Equinor in Porsgrunn, Norway, for their constant support and valuable guidance throughout the project. Their insightful comments and help have been crucial in shaping this thesis.

Last but not least, I extend my sincere thanks to my family and friends for their unlimited support and encouragement all the way from my country, Lebanon. I would also like to acknowledge the friendships and network I have built with my fellow students from diverse international backgrounds. The past two years of studying for my master's degree would not have been the same without their companionship.

Porsgrunn, May 15th, 2023

Mersal Al Halabi

Contents

List of Figures

List of Tables

1 Introduction

The first chapter of the thesis serves as an introduction to the research, outlining its background and objectives. Additionally, It outlines the various tasks that will be carried out throughout the thesis and finishes by defining the structure of the report.

1.1 Background and objective

Over the last two decades, the global demand for wind turbines has increased rapidly. Most of this demand has been driven by the necessity for "greener energy" electric power plants. Wind farms with multiple turbines are being built in the multi-megawatt range [1]. Wind farms are built both onshore and offshore based on wind availability, construction costs, and other dependencies or limitations to maximize wind power production or annual energy production (AEP). In 2021, 93% of the total 830 GW of installed wind capacity was onshore, with the remaining 7% being offshore wind farms. Onshore wind is a mature technology that is present in 115 countries worldwide, whereas offshore wind is still in its early stages of development, with the capacity present in only 19 countries [2]. However, as more countries develop or plan to develop their first offshore wind farms, offshore reach is expected to grow in the coming years due to both global decarbonization efforts and the increasingly competitive economics of offshore wind. Figure 1.1 shows the growth of offshore wind energy in the past years. The majority of the existing offshore wind capacity is in Europe, but there is a significant development in China, the United Kingdom, and elsewhere. A huge proportion of offshore wind projects are currently in the planning stages around the world.[3]

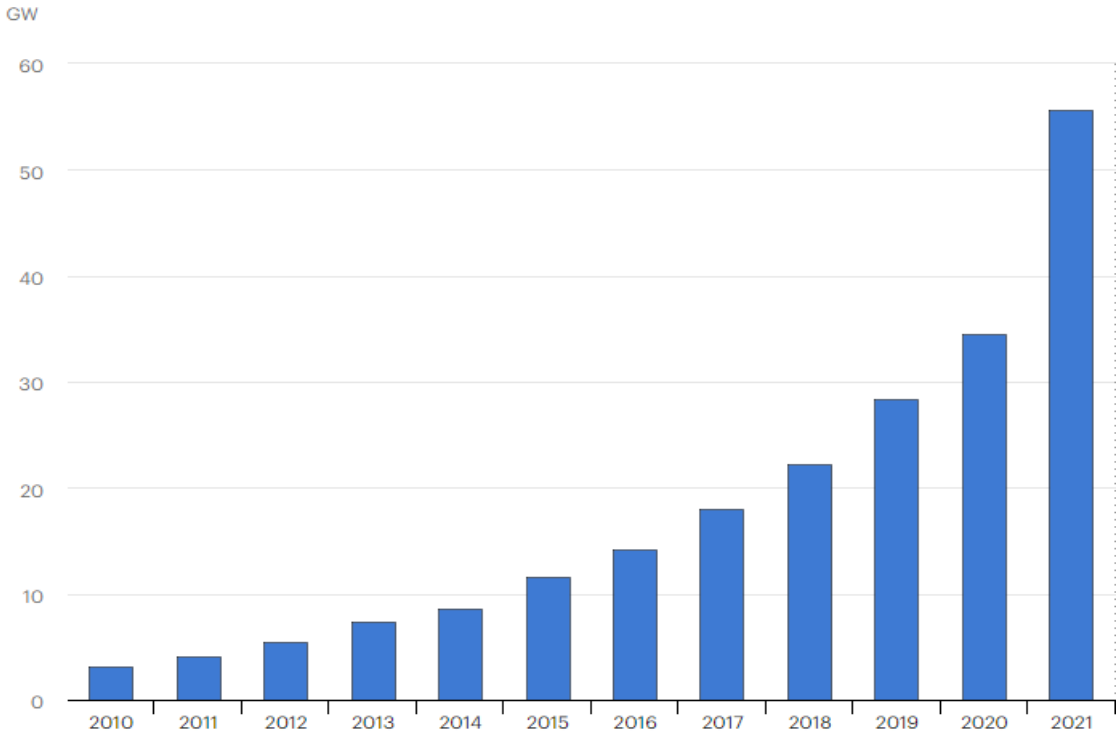

Figure 1.1: Global growth of offshore wind energy [2]

Teaming up wind turbines to form a wind farm might face some problems. One of these issues is wake loss, which occurs after the wind passes through the turbine's blades.[4] Seeing as wind turbines use wind energy to generate electricity, it stands to reason that the wind on the other side of the wind turbine has less energy. As a result, the wind downstream of the wind turbine is turbulent and has a reduced wind speed; this is known as the wind turbine's wake effect. [5]

Therefore, precisely modeling performance and estimating the annual energy production of wind farms while taking the wake effect into account in the early stages of the development is critical, as it has a significant impact on energy production, wind turbine life span, the success of wind energy projects as well as decreasing the CO2 emissions and enhancing the energy transition [6]. Computational Fluid Dynamics (CFD) can be used to evaluate wind farms. However, engineering models, such as those implemented in PyWake, are faster and thus more suitable when evaluating multiple design configurations [3].

In this work, wake effect simulations will be performed on Horns Rev 1 (described in Section 3.1), as it’s available in PyWake, with the wake being simulated using three different wake deficit models implemented in PyWake: N.O Jensen (NOJ), TurbOPark, and BastankhahGaussian. The objective is to determine which of the wake models produces the most accurate results when compared to the wind farm's measured data.

1.2 Thesis task description

The tasks required to accomplish this work are as follows:

1st task: Literature study and previous works, as well as a collection of offshore wind farm production data from public sources and publications.

2nd task: Choose the dataset.

3rd task: Run the PyWake simulator and compare simulated production to observed production using different wake models that should be tested for accuracy.

1.3 Report structure

The report has been structured in the following manner: In Chapter 2, a review of studies on wake effects in wind farms is presented, highlighting previous works that have utilized various wake models. Chapter 3 compares and outlines the features of several offshore wind farms located in the North Sea. The subsequent chapter, Chapter 4, offers a comprehensive explanation of the Pywake simulation tool, defines the wake effect, and details the three wake models that were utilized in this investigation. In Chapter 5, the results of the simulations are discussed and presented. The report concludes with Chapter 6, which provides a summary of the findings of this study.

2 Literature review

The upcoming chapter provides a literature review that showcases a variety of wake studies conducted within wind farms, along with past research that employed different wake models. The purpose of this review is to better understand the accomplishments of others in this particular domain.

2.1 Wake effect studies in wind farms

It is essential to consider the wake effect when designing a wind farm. This is because wake can reduce a wind farm's annual energy production (AEP), resulting in low wind energy production efficiencies. Thereby, studying the wake assists us in optimizing and evaluating the real capacity of wind farms. It is also important to have a look at what other researchers have done in this area and how they are measuring and estimating the wake losses in wind farms.

Jang-Oh Mo et al. investigated wake instability and its breakdown behind a wind turbine using a Large Eddy Simulation (LES) of an NREL (National Renewable Energy Laboratory) phase VI wind turbine inside a virtual wind tunnel with a section of 24.4 m by 36.6 m, using ANSYS FLUENT, a CFD software. They positioned the wind turbine approximately two rotor diameters upstream and twenty rotor diameters downstream. The simulation results were then compared to the experimental data posted by NREL, and no significant differences were discovered. They also noticed that the wake behind the wind turbine is made up of a network of intense and steady rotating helical vortices, then became unstable after some distance downstream of the wind turbine. The distance at which the instability occurs was later found to be a function of the upstream wind. For instance, when the upstream wind was 7m/s, the unsteady vortex structure appeared at four rotor diameters and full collapse occurred at six rotor diameters, however, when the upstream wind was increased to 15.1 m/s, the instability happened at eleven rotor diameters downstream and complete breakdown was seen two more rotor diameters further. Moreover, they found that the distance at which turbulence intensity (TI) decreases during the wake uncertainty and vortex breakdown process is also a function of upstream wind speed. Then, they used four different velocities, 7m/s, 10m/s, 13.1m/s, and 15.1 m/s, in order to determine the location of the boundary between the near and far wakes. [7]

In their study, D. Vahidi and F. Porté-Agel examined whether there is a scaling of the near distance from a wind turbine that leads to a collapse of the mean wake velocity shortfall under various ambient levels by performing an LES of the wake of a wind turbine under neutral atmospheric conditions with multiple turbulence levels. It was discovered that the higher the level of atmospheric turbulence, the faster the wake recovers and the shorter the near-wake length. They also looked into the potential of using the correlation obtained for the normalized optimum wake velocity deficit as a function of the normalized streamwise length in the sense of analytical wake modeling, taking two approaches: a) using the relationship as a stand-alone model to assess the maximum wake velocity deficit, and b) using the new relationship to calculate the wake advection velocity inside a physics-based wake expansion model. A good agreement between simulation data and model predictions was observed. [8]

R. J. Barthelmie et al. examined measurements from Denmark's Middelgrunden offshore wind farm, which has a curved-line shape of turbines placed 2.4 rotor diameter D apart, and discovered that average power losses due to wakes are approximately 10% of total production, with a down sequence turbulence intensity increase of 20%. [9]. In another work, R.J. Barthelmie and L. E. Jensen examined the consequences of wind distribution, atmospheric stability, and wind farm arrangement at the Nysted offshore wind farm in Denmark and concluded that wake losses are mostly linked to wind speed variation, whereas direction, atmospheric stability, and turbulence have second-order impacts. Besides that, wind farm efficiency is highly dependent on turbine spacing. [10]

De-Prada-Gil et al. conducted research on the possible advantages of a wind farm control strategy whose primary goal was to enhance total energy yield over its lifetime by taking into account that the wake effect in the wind farm differs based on the activity of each wind turbine. The research suggested that the control strategy optimizes the entire system by running some wind turbines at sub-optimal speeds. This was done to minimize the wake effect inside the wind farm and, as a result, maximize total energy production. This was done with two different wind roses. One wind rose was only at 90 degrees, while the other was at 30 degrees. The blade element momentum (BEM) theory is applied in the study. It moreover includes an in-depth wake model that takes into account single, partial, and multiple wake effects. The researchers noted that by employing the control strategy, the annual energy capacity of a wind farm could be increased from 1. 86% to 6.24%, by running specific wind turbines slightly off their ideal level and thus reducing the wake consequence.[11]

A wide range of analysis tools from the atmospheric science, economic and legal communities was used by J. K. Lundquist et al. in order to estimate the cost and implications of the wake effect generated by upwind wind farms. They also noticed that the wake could stretch to more than 50 kilometers downstream (behind the wind rotor), resulting in huge financial losses. [12]

Based on experimental data and field measurements, Li et al. evaluated the wake properties of a horizontal axis wind turbine (HAWT) in a wind farm. The HAWT generator has a 30kW capacity and a 10m rotor diameter. They began by measuring the reference wind speed and then reviewed the wake under various tip speed ratios and pitch angles at the turbine position x/D=2.0, where D is the rotor diameter. They then used the Gaussian function to foresee the wake model. As an outcome, the non-dimensional wind velocity ratio dropped as the pitch angle increased, and the full wake widths were seen at 0 degrees of pitch angle.[13]

2.2 Previous work using different wake models.

To better understand the behavior of the wakes forming behind the wind turbines as well as their effect on the AEP of a wind farm and other challenges they present, it is necessary to have some models to be used to simulate these wakes and estimate the energy production of wind farms. Several types of wake models are currently available and many more are expected in the near future. Below, some previous studies on different wake models will be presented.

Charhouni et al. looked into the effectiveness of three analytical wake models, Jensen, Ishihara, and Frandsen, in predicting wind velocity in the wake region using three criteria: parsimony, precision, and inaccuracy. As an outcome, it was discovered that the Jensen wake model was a very parsimonious model when compared to the two other wake models and that several factors taken into account have a significant influence on the accuracy of estimating velocity deficit. Nevertheless, the imprecision of the wake model was caused by the uncertainty on the trust level linked with some variable values, specifically, the trust coefficient and wake decay constant, which are related to wind farm characteristics. They also reached the conclusion that neither of the three analytical wake models can accurately estimate the wind velocity deficit, but the Jensen wake model, as per their research, is still the model that provides a good argument in terms of the three criteria.[14]

Three different wake models (Jensen wake model, 2D Jensen wake model, and Jensen-gaussian wake model) were utilized by Haiying Sun and Hongxing Yang to calculate Hong Kong's

offshore wind energy output. They also used the wake models to compare total electricity generation and power output from each wind turbine. The results revealed that the three wake models obtained no important differences in their total energy output estimations. After comparing the models, it was found that the Jensen wake model overestimates the power loss. Estimation errors for the 2D Jensen wake model and Jensen-Gaussian wake model were 1.55% and 0.38%, respectively, when compared to the Jensen wake model. Furthermore, they concluded that the wake model's influence on wind turbine structure is significant and warrants further investigation as it may indirectly affect the economic efficiency of wind farms.[15]

Göçmen et al. described six different wake modeling approaches developed at the Technical University of Denmark (DTU). Data from the Sexbierum onshore wind farm and the Lillgrund offshore wind farm were evaluated and compared to understand how to best utilize the models. The cases used illustrated that the Jensen model, the Larsen model, and Fuga are useful for large wind farm calculations because they are strong and computationally affordable, and they produced satisfactory results both onshore and offshore when the far wake region is taken into account and the atmospheric conditions are well defined. The CFD solvers, k–ε–f_P and LES, in particular, are found to be very nearly equal to the measurements. The study also demonstrates that introducing wind direction uncertainty improves the accuracy of the Jensen model, Larsen model, and Fuga power predictions for the Lillgrund wind farm case. Whereas, Even the most advanced model, Ellipsys3D LES, fails to replicate the depth of the wake deficit in the Sexbierum wind farm case.[16]

In their research, Shakoor et al. distinguished between the far and near wake effect in large wind farms. After comparing various far wake models on the basis of wake effect prediction and wind turbine power computation, it was deduced that Jensen's far wake model is an effective choice to solve the wind farm layout problem considering that it is simple and has a fairly high degree of accuracy. Also, they concluded that the prediction accuracy of all wake models is heavily influenced by the formatting and downstream distance between windmills in a wind farm. Upon studying the wind farm layout optimization problem, they discovered that more optimization techniques are needed to tackle the layout problem.[17]

Sadaghatizadeh et al. used numerical models to develop wind turbine wakes using LES, Jensen, Frandsen, 1st Larsen, and 2nd Larsen models. The models were validated with experimental data. In the investigation, the CFD program ICEM was used to generate a hexahedral mesh on the turbine blades in the cylindrical region. The researchers came to the conclusion that the

models overestimated the wake expansion while underestimating the velocity recovery rate. This could result in a wind farm with fewer wind turbines, producing less power. According to the researchers, the LES model can be used to obtain information about the flow field, which can then be used to plan a wind farm that operates under ideal circumstances.[18]

2.2.1 Studies using PyWake

Some previous research has been conducted using wake models implemented in PyWake, and since PyWake will be used in this thesis research, it is beneficial to look at these previous works and see how other researchers simulated wakes in wind farms.

Fischereit et al. compared, by simulations, a variety of wind farm models with varying complexity, fidelity, scale, and computational costs to Supervisory Control And Data Acquisition (SCADA). They selected two regional scale wind farm parameterizations implemented in the mesoscale Weather Research and Forecasting model (WRF), ExplicitWake Parameterization (EWP) and the wind Farm Parameterization (FIT), as well as 2 distinct high-resolution RANS simulations using PyWakeEllipSys installed with an actuator disk model, and three rapid engineering wake models from the PyWake suite. These models were utilized to wind farms of Nysted and Rødsand II, found in the Baltic Sea. They concluded that WRF+FIT using a resolution of 2 km is a good choice for capturing the average intra-farm variability in wind energy applications, whereas WRF+EWP was not efficient in estimating wind speed deficits. Besides that, they realized that all of the PyWake suite's engineering wake models simulate intra-farm wakes comparable to high-fidelity Reynolds-averaged Navier–Stokes (RANS) simulations, but they fail to accurately predict the farm wake effect of an upstream farm. According to their investigation, PyWakeEllipSys and WRF are found to be more accurate than PyWake for farm-to-farm wakes.[19]

Valotta Rodrigues et al. developed a surrogate model of Annual Energy Production (AEP) in PyWake for economic analysis methods for large offshore wind farms in their early stages of development, taking into account design spacing, turbine sizes, wind resource conditions, and farm layout arrangement. The model had a coefficient of accuracy of 0.994, indicating that it was a useful AEP calculator for financial evaluation. They observed that wind resources, turbine characteristics, and turbine number were more influential than the wind turbine spacing. However, keeping in mind the layout features (spacing) can improve the surrogate's exactness for economic analysis.[3]

Riva et al. optimized a wind farm design and operational techniques in both onshore and offshore applications using TOPFARM, a DTU wind energy software platform that includes a PyWake component. The goal was to allow the design of wind farms with limitations on Lifetime Damage Equivalent Loads (LDEL), where regions of the site and layouts that generate excessive loads could be excluded. With the addition of load constraints and the use of various types of surrogate models, quicker and more precise load predictions were obtained, while gradient-based optimization was enabled.[20]

Krabben et al. used two engineering wake models implemented in PyWake to evaluate wake losses in different offshore wind farms with curved and straight wind turbine rows. The NO Jensen model was the first engineering wake model used, followed by the Gaussian wake model. As an outcome, the curved wind farm layout has less fluctuation in energy supply than the rectangular wind farm layout since the curved wind farm's power generation is less reliant on wind direction than the rectangular wind farm layout. Their analysis showed that wind farms with curved rows outperform wind farms with straight rows.[21]

Van der Laan et al. suggest and use a simple wind speed independent actuator disk control method to decrease the number of iterations required and quicken the calculation of the annual energy production from RANS simulations of a 5×5 rectangular wind farm with 5 rotor diameter spacing using PyWake. By tilting the wind farm layout and using the new wind speed independent actuator disk control method, the effect of different wind directions and wind speeds are calculated sequentially in a single simulation. Since the global inflow wind speed and direction are kept constant, only local changes from a previously converged result must be reevaluated, and due to this, the total number of iterations is minimized by a factor of 2 to 3, and therefore, according to their finding, the wind speed independent actuator disk control method has the greatest chance of reducing the computation time of wind farm annual energy production calculations. [22]

3 Overview of offshore wind farms production data

The chapter showcases various offshore wind farms located in the Scandinavian region and their corresponding turbine production statistics that are collected from previous publications. The objective is to gain an overall understanding of the production performance of offshore wind turbines and select a wind farm for simulation using Pywake simulator and its implemented wake models.

3.1 Horns Rev 1

Horns Rev 1 is one of the wind farms that are already implemented in Pywake, together with its site specifications, wind speeds, and directions as well as its turbines.

3.1.1 Horns Rev 1 wind turbines and site specifications

Horns Rev 1 is a substantial offshore wind farm situated in a region with minimal turbulence. Its optimal configuration and position make it suitable for conducting comprehensive research on wake effects. With 80 Vestas V80-2000 wind turbines, it produces a total electricity capacity of 158 MW [23]. Each wind turbine at Horns Rev 1 possess a 2 MW energy capacity and stand at a hub height of 70 m with a rotor diameter of approximately 80 m. A visual representation of the turbine's dimensions can be observed in Figure 3.1.

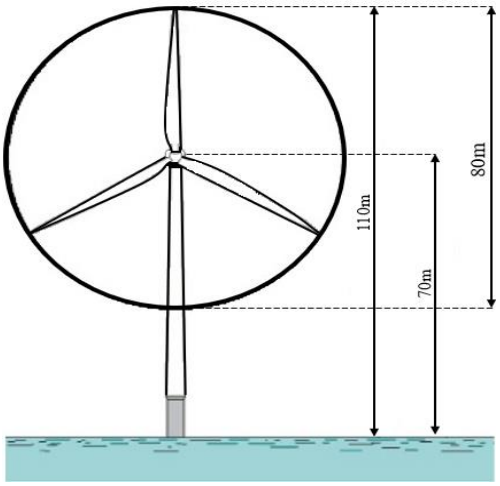

Figure 3.1: Vestas V80-2000 wind turbine dimensions.[24]

Horns Rev 1 is located in Denmark around 14 km far from the coast of the North Sea [25] as shown in Figure 3.2. At Horns Rev 1, wind speeds maintain an average velocity of 10 m/s facilitating optimal conditions for generating wind power. The water depth at the site varies between 6 to 14 meters. To ensure maximum capacity utilization, each wind turbine is placed 560 meters apart, equivalent to approximately 7 rotor diameters. The 80 wind turbines span over a 20-square-kilometer region and have been functional since 2002.[23]

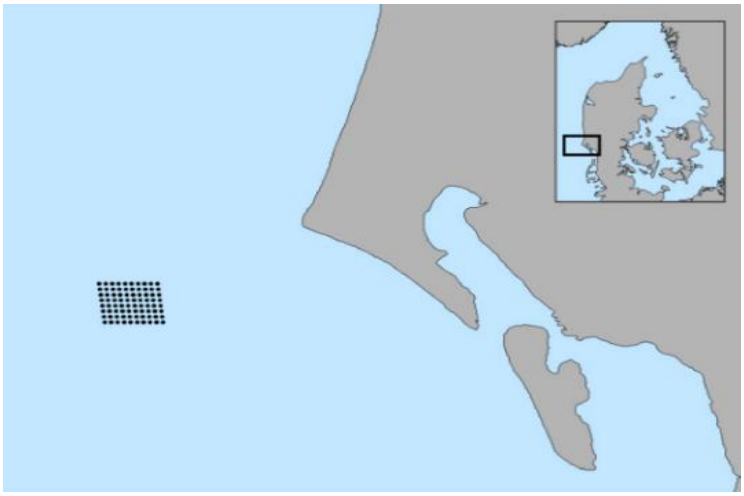

Figure 3.2: Horns Rev 1 location. [26]

Figure 3.3 illustrates the placement of three met masts surrounding the offshore wind farm, with the oldest mast named M2, which was established before the wind farm was constructed and was leveraged to assess the wind resource at the location. In the summer of 2003, the other two met masts (M6 and M7) were installed to study the recovery of wake flow behind the wind farm and to develop advanced scientific and technical models for computing wake effects from extensive offshore wind farms [24].

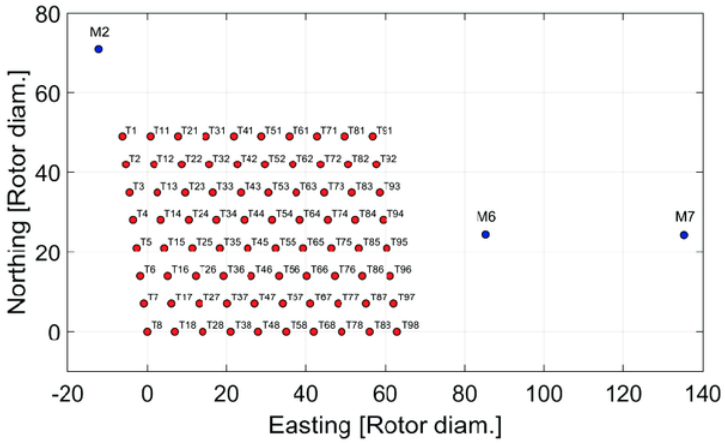

Figure 3.3: Installed met masts around Horns Rev 1 wind farm.[27]

Figure 3.4 below illustrates the wind distribution at Horns Rev 1 site, plotted with the Pywake simulator.

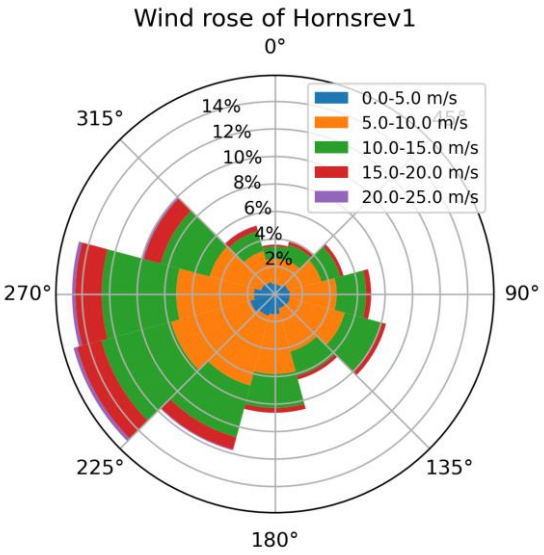

Figure 3.4: Wind Rose for the Horns Rev 1 site.

The wind rose chart illustrates the distribution of wind directions and corresponding wind speeds at the wind farm, by displaying the percentage of time that the wind blew from each direction. The above wind rose is divided into 8 sections with 45 degrees per section, and in each section, the wind velocity is divided into 5 ranges with each of interval 5 m/s. According to the chart, the wind blew from the 270˚ direction for approximately 15% of the time, and from the [55˚- 90˚] direction for roughly 7% of the time.

3.1.2 Horns Rev 1 turbine power data

As previously stated, the wind turbines utilized at the Horns Rev 1 offshore wind farm are the Vestas V80-2000 model. Table 3.1 depicts the power output and thrust coefficient of an individual wind turbine at various wind speeds.

Table 3.1: Electric power and thrust coefficient of Vestas-V80-2000 wind turbine.[24]

Wind Speed	Electric Power (kW)	Thrust Coefficient	Wind Speed	Electric Power (kW)	Thrust Coefficient
4	66.6	0.818	15	1997	0.249
5	154	0.806	16	1999	0.202
6	282	0.804	17	2000	0.167
7	460	0.805	18	2000	0.14
8	696	0.806	19	2000	0.119
9	996	0.807	20	2000	0.102
10	1341	0.793	21	2000	0.088
11	1661	0.739	22	2000	0.077
12	1866	0.709	23	2000	0.067
13	1958	0.409	24	2000	0.06
14	1988	0.314	25	2000	0.053

The Electric power as well as the thrust coefficient are plotted against the wind speed and can be seen in Figure 3.5, below.

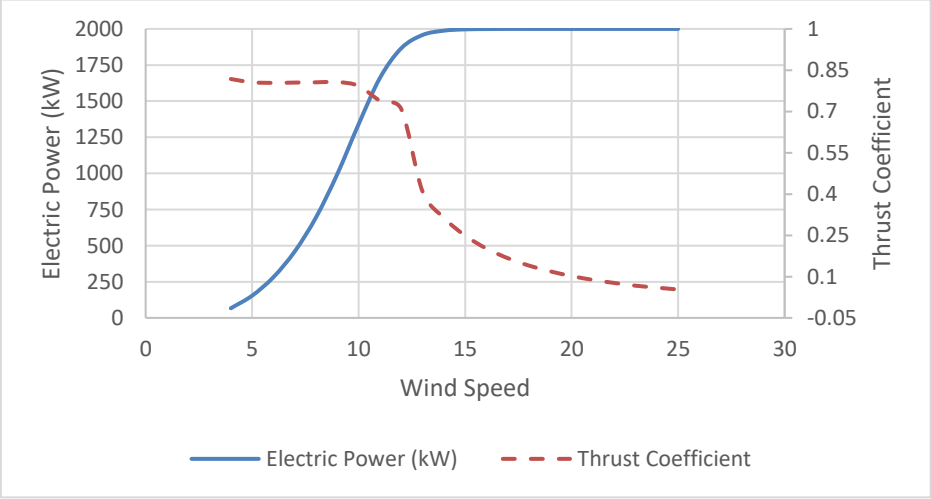

Figure 3.5: Vestas-V80-2000 nominal power generation and thrust coefficient as a function of the wind speed.

3.2 Lillgrund wind farm

Lillgrund farm, has also been integrated into PyWake along with its turbines and sites.

3.2.1 Lillgrund location and wind turbine description

Lillgrund offshore wind farm is located in the Baltic Sea, it is far from the Swedish and Danish coasts around 7 and 9 km, respectively, as seen in Figure 3.6. It is Sweden's largest offshore wind farm and the third largest worldwide. Each year, around 330 GWh of electricity is generated from the wind farm, supplying not less than 60,000 houses in Sweden. [28]

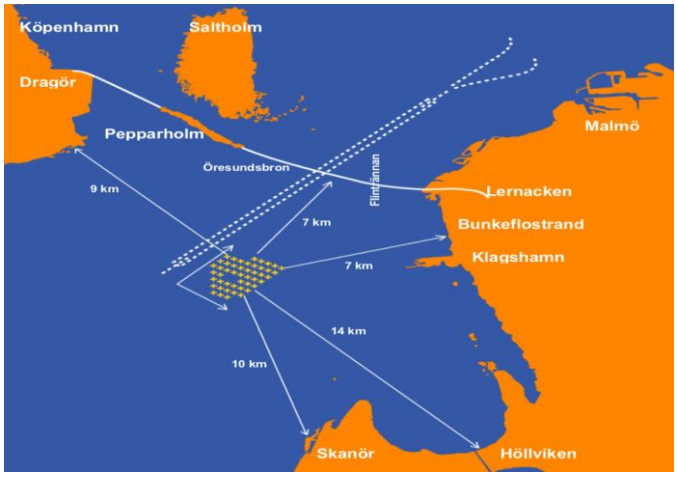

Figure 3.6: Lillgrund wind farm location and layout. [29]

Lillgrund farm has 48 wind turbines of type Siemens SWT-2.3-93. It has a larger rotor diameter (93 m) than that of Horns Rev 1 turbine (80 m), as well as a higher hub height of 80 m. A drawing of the turbine is shown in Figure 3.7 with the dimensions.

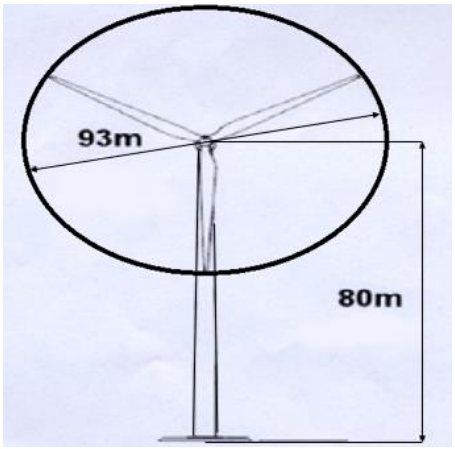

Figure 3.7: Schematic representation of Siemens SWT-2.3-93 wind turbine.[30]

The wind rose of Lillgrund wind farm is plotted in PyWake, and presented in Figure 3.8 below:

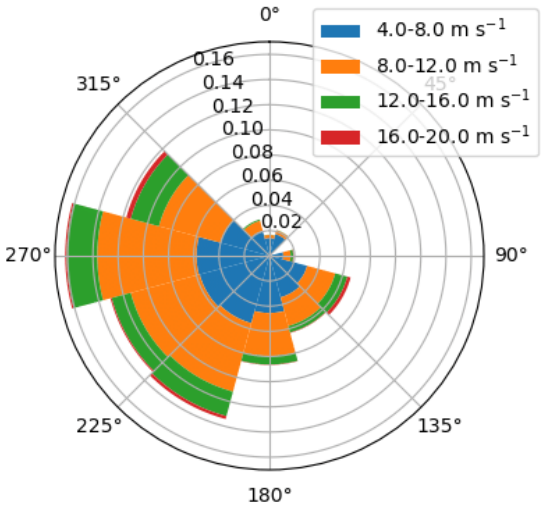

Figure 3.8: Wind rose at the Lillgrund site.

3.2.2 Lillgrund turbine power data

The Siemens SWT-2.3-93 turbine has a rated power output of 2300 kW and is designed to operate efficiently in a wind speed range of 4 m/s to 25 m/s. Table 3.2 shows the power data for the Siemens SWT-2.3-93.

Table 3.2: The electric power of Siemens SWT-2.3-93 turbine at different wind speeds. [31]

Wind Speed	Electric Power (kW)	Wind Speed	Electric Power (kW)
4	65	15	2299
5	180	16	2300
6	352	17	2300
7	590	18	2300
8	906	19	2300
9	1308	20	2300
10	1767	21	2300
11	2085	22	2300
12	2234	23	2300
13	2283	24	2300
14	2296	25	2300

The power curve, which illustrates the relationship between wind speed and power output, can be found in Figure 3.9. It is worth noting that the cut-in and cut-off wind speeds indicate the minimum and maximum wind speeds at which the turbine can start generating power and must shut down, respectively. This information is crucial for understanding the turbine's performance and ensuring its safe operation.

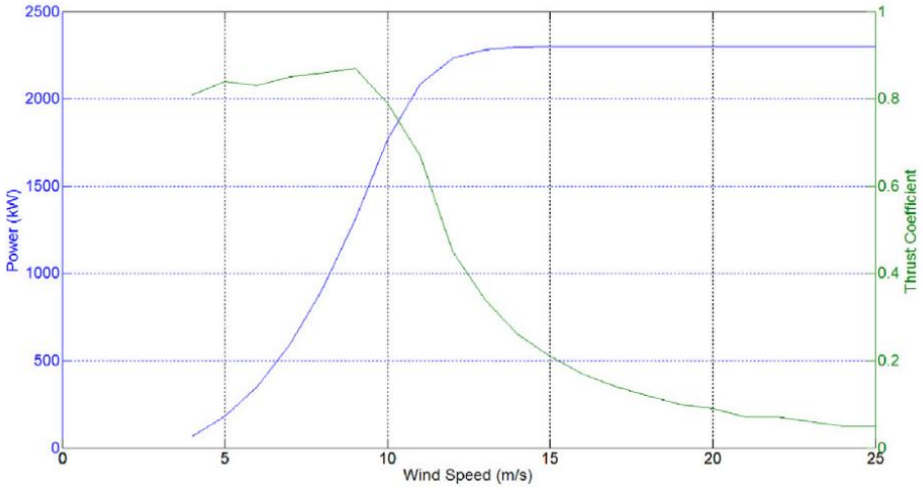

Figure 3.9: Thrust coefficient and power curve for Siemens SWT-2.3-93. [32]

3.3 Nysted wind farm

Unlike the two previously mentioned wind farms, Nysted wind farm has not been included yet in Pywake libraries.

3.3.1 Nysted location and wind turbines

The farm is considered one of the largest of its kind, and it is located off the coast of Denmark, around 11km to the south of Nysted town in the island of Lolland in the Baltic Sea, Figure 3.10. This location was chosen due to the favorable wind conditions in the area, which are ideal for generating electricity from wind power. The farm has been recognized for its contribution to the reduction of carbon emissions and transition to renewable energy, as well as it played an important role in making Denmark a leader in the green shift.

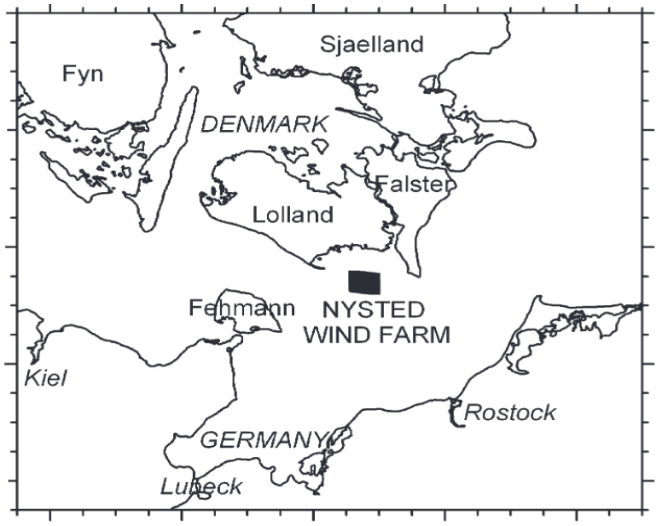

Figure 3.10: Location of Nysted wind farm [10]

Nysted wind farm was officially commissioned in December 2003. It has a total of 72 wind turbines of type Bonus 2.3 MW, each with a capacity of 2.3 MW, which is the same capacity as the wind turbine, Siemens SWT-2.3-93, of Lillgrund wind farm. The turbines of Nysted wind farm are situated in relatively shallow waters, with a depth between 6 and 10 m [33], which makes installation and maintenance of the turbines easier and more cost-effective. These turbines have 82.4 m rotor diameter and a hub height of 69 m as presented in Figure 3.11.

Figure 3.11: Bonus 2.3 MW dimensions. [34]

The distribution of wind speed over 5 m/s at the Nysted site, under different directions is displayed in Figure 3.12.

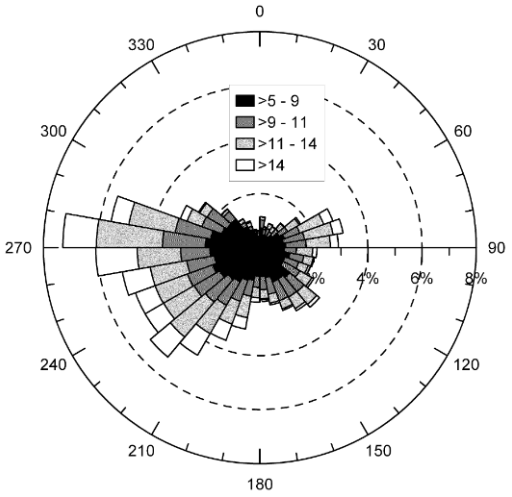

Figure 3.12: Wind Rose at Nysted wind farm site [10]

3.3.2 Wind turbine power and thrust coefficient curves.

As previously stated, the Bonus 2.3 MW wind turbine is employed in the Nysted wind farm, capable of producing 2300 kW and designed to operate at a rated wind speed of 25 m/s. The turbine initiates power generation at a wind speed of 3.5 m/s and ceases at 25 m/s, however, it can endure wind speeds up to 55 m/s. Figure 3.13 displays both the power curve and the thrust coefficient curve for the Bonus 2.3 MW turbine, providing a visual representation of the turbine's performance characteristics. It is worth noting that these curves are critical in determining the optimal operating conditions of the turbine and ensuring its maximum efficiency.

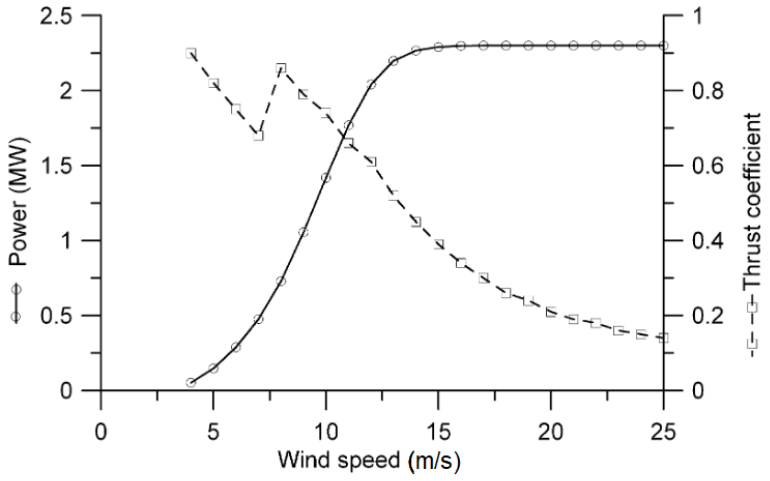

Figure 3.13: Power and thrust coefficient curves of Bonus 2.3 MW turbine [10]

The overall capacity of Nysted wind farm is around 165.6 MW, and the annual energy output of the farm is 595 GWh, which is equivalent to the electricity consumption of roughly 145,000 households over the course of a year. This highlights the significant contribution of the wind farm in meeting the energy needs of many households.[35]

3.4 Hywind wind farm

The Pywake libraries lack implementation of the Hywind offshore wind farm site and wind turbine objects, requiring them to be defined before simulations can be conducted on this wind farm.

3.4.1 Hywind site and turbine

Located in the North Sea off the coast of Scotland, Figure 3.14, Hywind is a floating offshore wind farm that was developed by Equinor (previously known as Statoil). As of now, it is the only floating offshore wind farm in the world, covering an area of approximately 4 square kilometers and providing electricity to around 20,000 homes in the UK. Since it began operating in October 2017, it has demonstrated the potential of floating offshore wind farms by achieving the highest average capacity factor among all UK offshore wind farms [36].

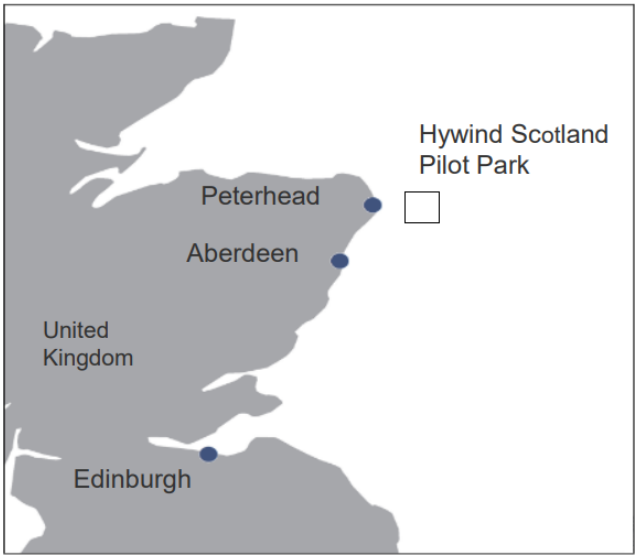

Figure 3.14: location of Hywind offshore wind farm. [37]

The wind conditions at the Hywind offshore wind farm site are generally considered to be favorable for wind energy generation. The North Sea is known for its strong and consistent

winds, which make it a prime location for offshore wind farms. The average wind speed at the site is around 10 meters per second (m/s), or approximately 22 miles per hour. However, wind speeds can vary depending on the time of year and weather conditions. The turbines at Hywind are designed to operate in wind speeds of up to 60-70 m/s, which are relatively high compared to some other offshore wind farms like the previous farms presented [38].

In addition to the wind speed, wind direction is also an important factor in determining the performance of wind turbines. Overall, the wind conditions at the Hywind offshore wind farm site are considered to be suitable for wind energy generation. Figure 3.15, displays the wind rose at Hywind Scotland wind farm site.

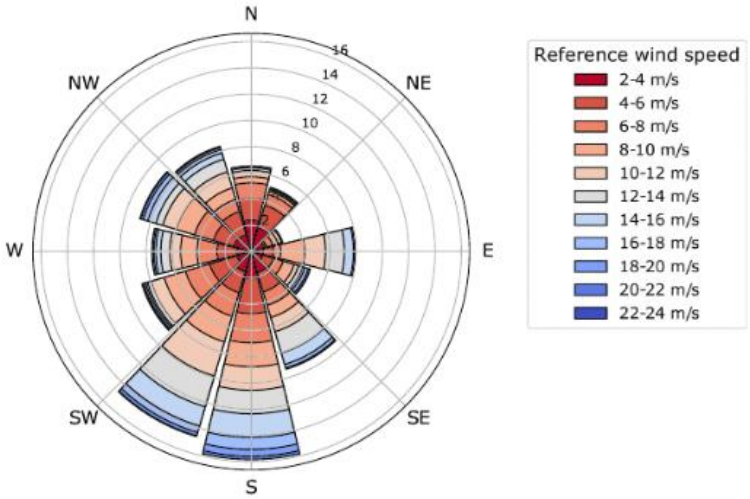

Figure 3.15: Wind rose at Hywind Scotland site. [39]

3.4.2 Turbine specifications

Hywind offshore wind farm consists of five floating wind turbines of the type Siemens SWT-6.0-154, which are anchored to the seabed by mooring lines. Each of the turbines at Hywind has a capacity of 6 megawatts (MW), giving the entire farm a total capacity of 30 MW. The rotor diameter of each turbine is 154 meters, and the hub height is 98 meters above sea level. As the wind speed are high at the farm's site, the turbines at Hywind are designed to rotate to face the wind direction, which allows them to capture as much energy as possible from the wind, they are equipped with blades that can adjust their pitch angle to optimize their performance in changing wind conditions. [38]

The specifications of the wind turbine at Hywind farm, along with the layout of the turbines in the farm, are presented in Figure 3.16.

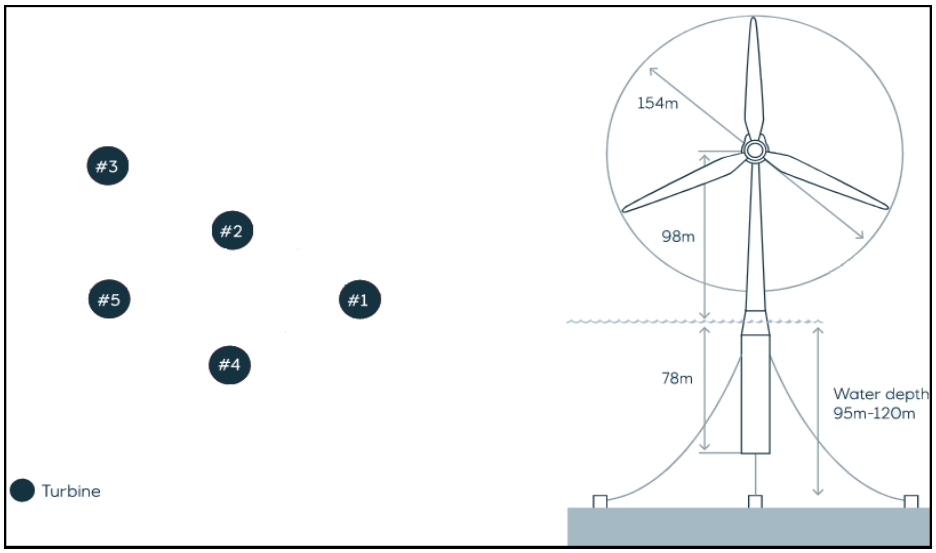

Figure 3.16: Hywind's turbine specification and layout. [36]

The Siemens SWT-6.0-154 begins generating electricity when the wind speed reaches 3.5 m/s and ceases at 25 m/s. Its rated wind speed is 13 m/s. However, it has the ability to endure high wind speeds without suffering mechanical damage, as previously stated. Table 3.3 presents the turbine's power in tabular form, while Figure 3.17 depicts it graphically against wind speed together with the thrust coefficient of the turbine [40].

Table 3.3: Electric power of Siemens SWT-6.0-154 [41]

Wind Speed	Electric Power (kW)	Wind Speed	Electric Power (kW)
3.5	200	14.5	6000
4.5	320	15.5	6000
5.5	575	16.5	6000
6.5	945	17.5	6000
7.5	1485	18.5	6000
8.5	2157	19.5	6000
9.5	2940	20.5	6000
10.5	3930	21.5	6000
11.5	5160	22.5	6000
12.5	5960	23.5	6000
13.5	6000	24.5	6000

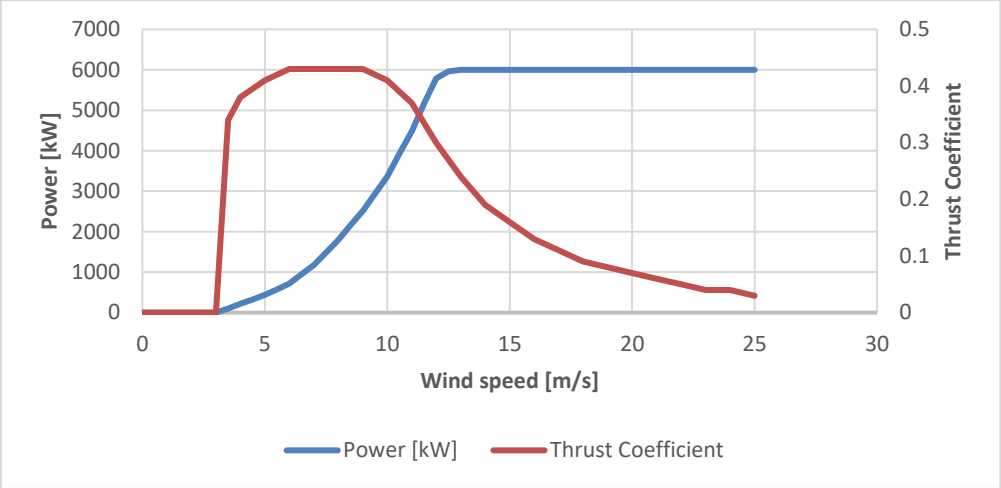

Figure 3.17: Power curve and thrust coefficient against wind speed in m/s for Hywind's farm wind turbine, Siemens SWT-6.0-154.

3.5 Wind farms' summary

Wind turbines typically exhibit a consistent power curve shape, as seen in the cases of Vestas-V80, SWT-2.3-93, Bonus 2.3 MW, and Siemens SWT-6.0-154 turbines, but the specific values of the power of wind turbines and the cut-in and cut-off speeds can vary. Similarly, the thrust coefficient curves for these turbines may also differ in their values and characteristics. It is important to note that these differences have the potential to impact the overall performance and efficiency of not only the individual turbines but also the entire wind farm. Additionally, the power curve and thrust coefficient curves of wind turbines are affected by a range of factors such as wind speed, air density, and blade pitch angle. These curves are important in determining the optimal operating conditions of a turbine and maximizing its energy output. Understanding the variation of these curves is crucial for engineers and operators in the wind power industry to make informed decisions regarding turbine design, placement, and maintenance. By analyzing and optimizing these curves, the efficiency and productivity of wind turbines can be improved, making wind energy an even more viable and sustainable source of power.

3.6 Choosing windfarm and dataset

The aim of this thesis was to conduct a comparative analysis of production data from wind farms, with a specific focus on offshore wind farms. The reason why the four wind farms mentioned in this chapter were chosen is because they are situated in the North Sea and the Scandinavian region, where offshore wind energy is rapidly expanding. However, it should be noted that the actual power production data of these offshore wind farms is considered confidential and requires the signing of confidentiality agreements, making it inaccessible to the public, and due to the limited time available, obtaining such agreements may be difficult.

The selected offshore wind farm for this study is Horns Rev 1, described in Section 3.1. The selection of the Horns Rev 1 offshore wind farm was based on several factors, including the availability of real power data collected from previous studies that have simulated this wind farm. By utilizing this real data, the accuracy and reliability of the results obtained from this study can be improved. Another reason for selecting Horns Rev 1 is its inclusion in Pywake libraries, which provides a pre-existing model of the wind turbines (Vestas-V80) and the site specifications and wind conditions there, streamlining the process of implementing the wind farm object and site. As the timeline for this thesis work is tight, utilizing an existing model instead of building one from scratch can save precious time and resources.

The real data used in this study were collected from previous publications, such as the works of Barthelme et al., 2010 [42] and Pena et al. [43], which serve as valuable references for this study.

4 Pywake, wake effect and wake models definitions

This chapter provides a brief definition and description of Pywake's usage. It also explores the impact of wake effect on wind energy and how it affects the energy production in wind farms. Additionally, the three wake models used in this thesis work are numerically described along with their consideration of the wake after the wind turbine.

4.1 PyWake

PyWake is a Python-based accessible wind farm simulation tool developed at DTU that can compute flow fields, the power production of individual turbines, as well as annual energy production (AEP) of a wind farm while considering wake losses using a variety of engineering wake models implemented in Python, as well as CDF RANS. The reason behind choosing is that it is incredibly effective at estimating how wake propagates within a wind farm and can evaluate turbine interaction using different formats of wind resource data, in addition to its capability of visualizing flow maps for the wind farm’s layout in the study [44]. Moreover, it is a relatively fast tool and can handle more than one variable at a time.

PyWake’s architecture is shown in Figure 4.1. The WindFarmModel, which is created with a Site and a WindTurbines object, is the primary object in PyWake's architecture. It returns a SimulationResult object with the results of the calculated effective wind speed, power output, and thrust coefficient of each turbine. Furthermore, it is based on methods for calculating AEP and generating flow maps for entire wind farms.

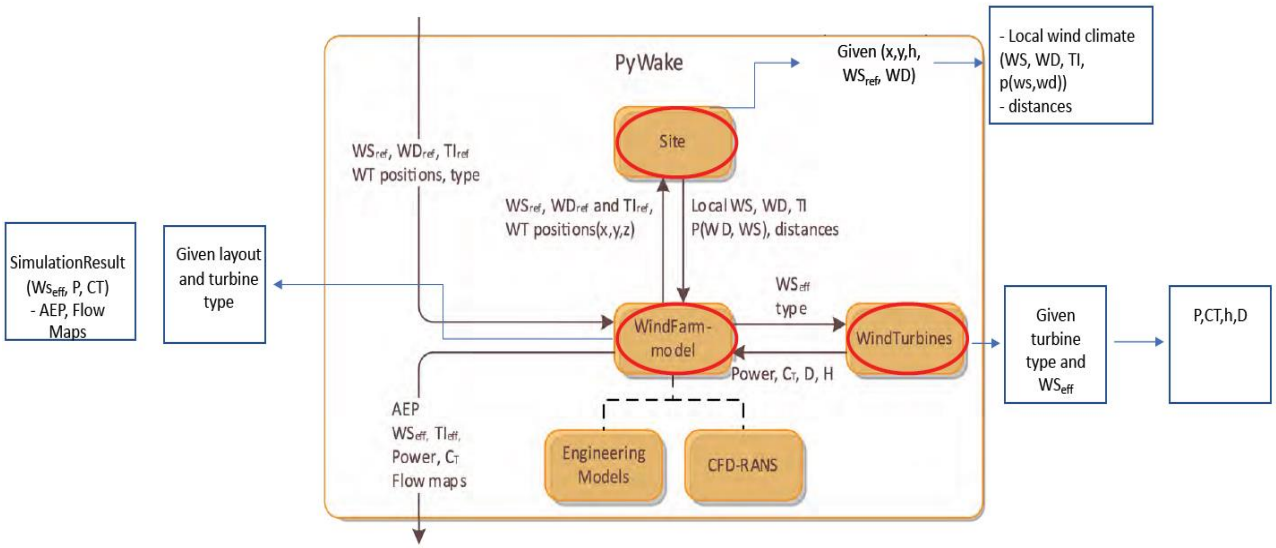

Figure 4.1: PyWake architecture [45]

The Site object characterizes the wind conditions at a specific location, including parameters such as wind speed (WS), wind direction (WD), turbulence intensity (TI), as well as the likelihood of specific wind speed and direction combinations based on the turbine position (x.y), reference wind speed (WSref), and wind direction (WDref).. The Site object is also in charge of calculating the downwind, crosswind, and vertical distance between wind turbines. The WindTurbines object, on the other hand, gives the power curve, thrust coefficient (CT) curve, as well as the hub height (h) and diameter of the wind turbine (D).

4.2 Wake effect

Wake is viewed as a significant issue affecting wind energy generation. Wake is created by the turbulent flow of wind after it passes through the wind turbine rotor, i.e., downstream of the wind turbine. The wake generated by a single wind turbine can cause a drop in wind speed, reducing the amount of energy that can be extracted from the wind. This turbulent flow is primarily caused by the dynamics of vortices generated by the rotor blades. In a wind cluster, wakes from multiple wind turbines can interact with one another and create undesirable effects. When wakes overlap, they can lead to a rise in turbulence intensity, causing an increase in dynamic loadings on downstream wind turbines. This increase in turbulence intensity can also result in unwanted blade vibrations, which can cause fatigue damage to the structural components of the turbine. As a result, the wind energy generated by downstream turbines is reduced, impacting the overall efficiency and productivity of the wind farm. [46]

The growth of the wake after a wind turbine is illustrated in Figure 4.2.

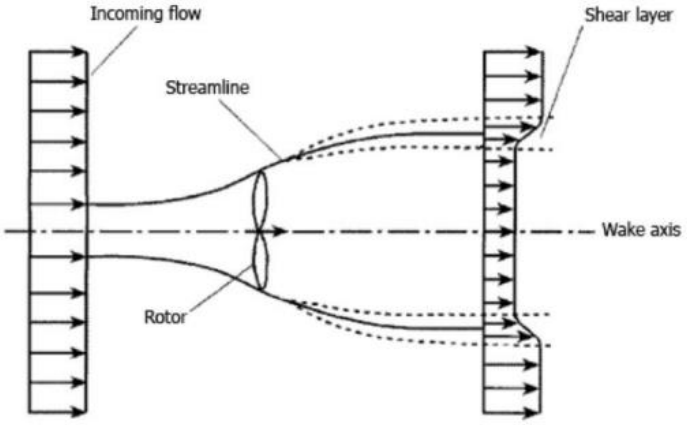

Figure 4.2: Axisymmetric flow-based wake growth [47]

A wind turbine's wake can be classified into three regions: near wake, intermediate wake, and far wake. The near wake is generally defined as the area right behind the rotor and can be seen up to 2 rotor diameters downstream, obviously, it depends on the incoming flow [48]. The intermediate wake lies between the near and far wakes at around 3 to 5 rotor diameters downstream of the wind turbine. The far wake, on the other hand, is the region further than 6 rotor diameters, Figure 4.3. Due to the fact that far wakes have a greater influence on downstream wind turbine energy production, the focus should be more on far wakes instead of near wakes when designing a wind farm. When considering the performance and physical process of power extraction, then a near wake is critical.

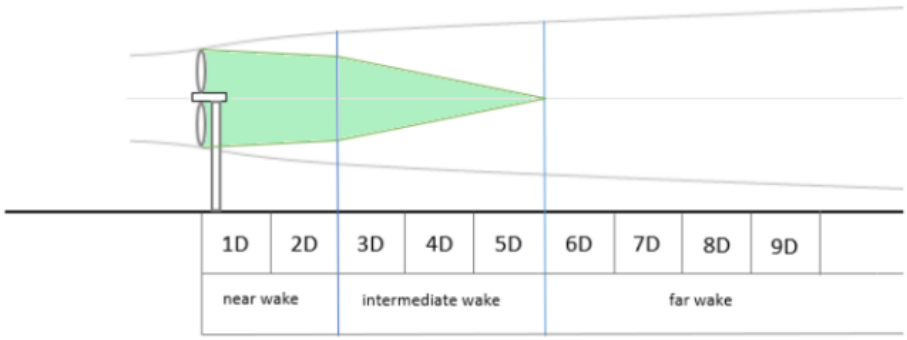

Figure 4.3: Illustration of near, intermediate, and far wake regions with respect to the wind turbine [49].

4.3 Wake models

4.3.1 N.O. Jensen (NOJ)

The N.O. Jensen's wake model was created in 1983 and is regarded as a simple wake model [33]. Since the near field behind the wind turbine is ignored in this model, the resulting wake behind the generator is treated as turbulent, implying that this wake model is only strictly applicable in the far wake region. Furthermore, the wake behind the wind turbine expands linearly, and the velocity deficit is only affected by the distance downstream of the turbine. Based on their research, Duckwork et al. [34] recommended using N.O. Jensen's model for energy production in offshore wind farms because it obtained small errors when compared to experimental data. The model is derived from applying the law of conservation of momentum for wind turbines as shown in equation 4.1. [50]

$$\pi r_t^2 v + \pi(r^2 - r_t^2)v_0 = \pi r_c^2 v_1 \tag{4.1}$$

In the above equation, v stands for the wake speed just behind the turbine, v_0 is the free stream wind speed entering the wind turbine, r_t denotes the wind turbine's rotor radius, r_c and v_1 represent the wake radius and wake velocity at the downwind distance x, respectively.

When solving equation 4.1, with respect to the velocity, a relationship between the downstream velocity and the upstream one can be obtained. And according to Betz's theory, the relation can be seen in equation 4.2 [17]:

$$v = (1 - 2a)v_0 \tag{4.2}$$

Where a is the axial flow induction factor.

Based on the assumption of linear expansion of the wake, the wind follows a conical shape behind the wind turbine's rotor, and the radius, r_c, of this conical shape can be estimated using equation 4.3:

$$r_c = r_t + \alpha x \tag{4.3}$$

Where α (or k_w in some articles) is a dimensionless scalar that determines the rate at which the wake grows with the distance, and usually taken as 0.04 for offshore wind farms [21], and it is defined as:

$$\alpha = \frac{1}{2}\ln\left(\frac{h}{z_0}\right) \tag{4.4}$$

Here, h is the wind turbine's hub height, and z_0 represents the surface roughness of the wind farm and depends on the location of the wind farm.

Equation 4.5 shows how to compute the speed in the wake area, or wake velocity, at a distance x from the wind turbine as a function of the incoming free stream wind speed; however, this velocity function is imprecise in the near wake area and can only be used in far wake regions, which are at about 6-8D in offshore wind farms.

$$v_1 = v_0 + v_0\left(\sqrt{1 - C_T} - 1\right)\left(\frac{r_t}{r_c}\right) \tag{4.5}$$

In the fully developed regime, this velocity is given by:

$$v_1 = v_0\left[1 - \frac{1 - \sqrt{1 - C_T}}{(1 + 2\alpha s)^2}\right]\pi r_c^2 \tag{4.6}$$

Where, C_T is the thrust coefficient of the upwind turbine and a function of the induction factor a,computed from the turbine characteristics curve [47]. s is a function of the wake location, $s = x/2r_c$. In the case where $s = 0$, i.e., just behind the rotor, the velocity equation becomes:

$$v_{1_{(s=0)}} = v_0\sqrt{1 - C_T} \tag{4.7}$$

Figure 4.4 shows the concept of the single wake Jensen model assuming linear expansion of the wake cone.

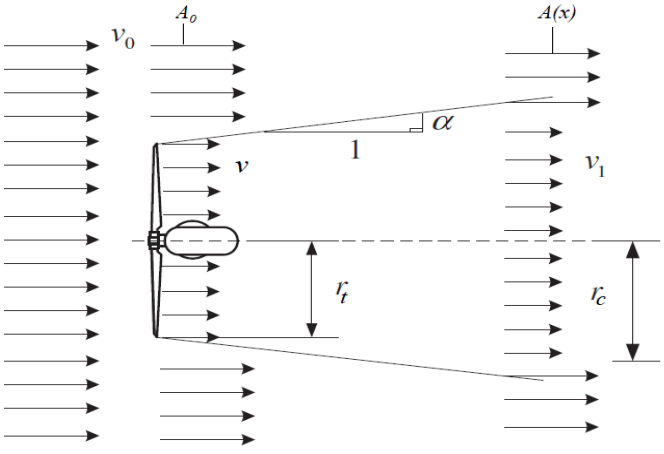

Figure 4.4: Wake shape assumption by Jensen wake model [5]

4.3.2 TurbOpark

The TurbOpark wake model (Turbulence Optimized Park Model) is a popular model in offshore wind farm simulations for predicting wind turbine wake characteristics. [51] The model includes additional features, such as the wake expansion, to better represent wake behavior in real-world wind farms, it assumes that the wake expands with distance downstream from the turbine in a Gaussian manner, but it differs from other analytical models in its definition of the wake expansion by using a non-linear streamwise wake expression rather than the more commonly used linear expansion. The model also takes into account how atmospheric turbulence affects the wake. The TurbOpark model requires inputs such as the diameter of the turbine rotor, the height of the hub, the wind speed and direction, and the intensity of atmospheric turbulence.[52]

TurbOpark is implemented in Pywake and is employed in two different configurations: one represents the original model by Nygaard et al, [51], and the other is a revised configuration in which the ground model for the wake deficit is turned off and a wake expansion coefficient B of 0.06 is used instead of 0.04. [52]

The wake growth rate, $\frac{dD_w}{dx}$, equation 4.8, is a function of the turbulence intensity, I_x, in the wake and a wake expansion coefficient B.

$$\frac{dD_w}{dx} = BI_x \tag{4.8}$$

The turbulence intensity is a function of the atmospheric turbulence intensity, I_{atm} , and the additional turbulence intensity generated in the wake, $I_{w,x}$, as shown in equation 4.9.

$$I_x = \sqrt{{I_{atm}}^2 + {I_{w,x}}^2} \tag{4.9}$$

Where the additional turbulence is described as:

$$I_{w,x} = \frac{1}{c_1 + c_2 \frac{x}{D\sqrt{C_T v}}} \tag{4.10}$$

c_1 and c_2 are two constants given as 1.5 and 0.8, respectively [52], v is the incoming wind speed, and D is the rotor diameter.

With increasing downstream distance, the combined turbulence intensity approaches the ambient atmospheric turbulence intensity. As a result, the wake expands fastest closest to the turbine, where the wake contribution to turbulence is greatest. The wake expansion slows down further downstream, eventually reaching a linear expansion at a constant rate. The width of the wake at a specific downstream distance can be found using the analytical expression 4.11.

$$D_{w,x} = D + \frac{BI_{atm}D}{\beta}\left\{\sqrt{\left(\alpha + {\beta x}/{D}\right)^2 + 1} - \sqrt{1+\alpha^2} - ln\left[\frac{\left(\sqrt{\left(\alpha + {\beta x}/{D}\right)^2 + 1} + 1\right)\alpha}{\left(\sqrt{1+\alpha^2}+1\right)\left(\alpha + {\beta x}/{D}\right)}\right]\right\} \quad (4.11)$$

Here, α and β are two auxiliary positive variables introduced, where $\alpha = c_1 I_{atm}$, and $\beta = \frac{c_2 I_{atm}}{\sqrt{c_T v}}$.

4.3.3 BastankhahGaussian

The BastankhahGaussian wake model is another model used in wind energy for predicting wind speed deficits caused by wind turbines. The model was first introduced by Majid Bastankhah in 2016 [53].

The model assumes that a wind turbine's wake can be approximated as a Gaussian distribution (also known as the normal distribution) of wind speed deficits, thus the velocity deficit in the turbine wake has a gaussian shape regardless of the incoming conditions, as seen in Figure 4.5, below.

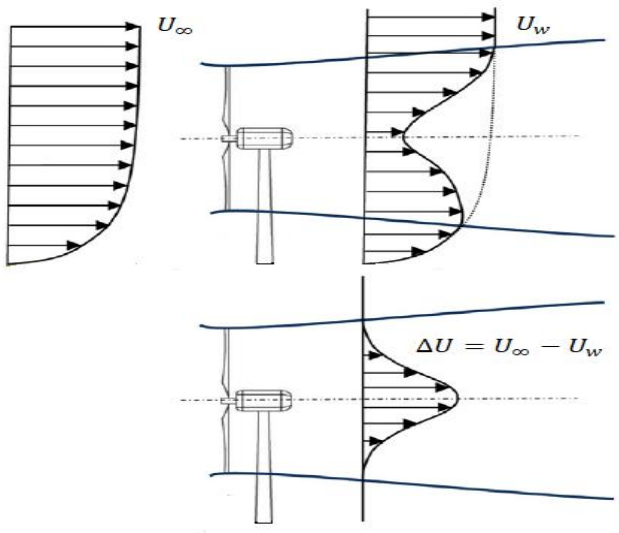

Figure 4.5: Gaussian distribution of the velocity deficit in the wake area [53].

The wind speed and direction, turbine diameter, distance between turbines, and the ambient turbulence intensity are all factors considered by the model. The wake velocity in the x-direction, U_w, according to this model is given by:

$$U_w = U_\infty \left(1 - C_x exp^{-\frac{r^2}{2\sigma^2}}\right) \tag{4.12}$$

Where, U_∞ is the free stream wind velocity entering the turbine, and C_x (equation 4.13) stands for the maximum normalized velocity deficit at each downstream location that occurs at the center of the wake, r identifies the wake radius, and σ represents the standard deviation of the Gaussian-shaped velocity profiles at each distance x downstream the rotor.

$$C_x = 1 - \sqrt{1 - \frac{C_T}{8(\sigma/D)^2}} \tag{4.13}$$

Here, C_T and D are the thrust coefficient and the wind turbine diameter, respectively.

The BastankhahGaussian model introduces a different coefficient from the Jensen model, which is the growth rate of the wake, k^*, which is based on the turbulence intensity, $k^* = 0.003678 + 0.3837I_a$. The standard deviation σ is a function of the growth rate and can be calculated using equation 4.14 [54].

$$\sigma = k^* x + D\varepsilon \tag{4.14}$$

ε denotes the value of σ/D as x reaches zero.

Now, the velocity deficit according to the BastankhahGaussian model can be formulated from equation 4.12, taking $\Delta U = U_\infty - U_w$, is written as:

$$\frac{\Delta U}{U_\infty} = \left(1 - \sqrt{1 - \frac{C_T}{8(\sigma/D)^2}}\right) exp^{-\frac{r^2}{2\sigma^2}} \tag{4.15}$$

The value of ε should be calculated before utilizing equation 4.14, and this can be done by calculating the total mass flow rate at $x = 0$. The velocity profile cannot be predicted accurately at $x = 0$, since it is assumed to have a uniform distribution and then changes to a Guassian profile.

5 Results and Discussion

The upcoming chapter presents the outcomes of power generation simulations conducted at the offshore wind farm Horns Rev 1. The purpose of the simulation study is to demonstrate that the wake models implemented in Pywake tool are suitable for studying wake effects on power production of offshore wind farms. These simulations involved using three wake models: NOJ, BastankhahGaussian, and TurbOPark, that are implemented in the Pywake simulator in Python. However, it is crutial to mention that default parameters of these models where used in the simulation.

Real data obtained from earlier studies by Pena et al. [43] (First data case) and Barthelmie et al. [42] (Second data case) on Horns Rev1 were employed in the analysis to validate the accuracy of the models. The simulations were carried out considering various wind directional bands, which were selected based on the availability of real data to compare the simulated results. The average wind speed at Horns Rev1 varies between 8 and 10 m/s, and since both Pena et al. and Barthelmie et al. used 8m/s as the wind speed in their studies, it remains unchanged in this study so that the results can be compared with the real data..

5.1 Power and Thrust coefficient of Vestas V80 using Pywake.

The real power and the real thrust coefficient of the Vestas V80-2000 wind turbine were compared with the simulated values at various wind speeds using the Pywake simulator in Python. The results of this analysis are presented in Figure 5.1. The data utilized for this chart were sourced from the research paper by Leo E. Jensen et al. [24],which presents a compelling example of the insights that can be obtained from the SCADA system and the met masts (M2, M6, and M7).

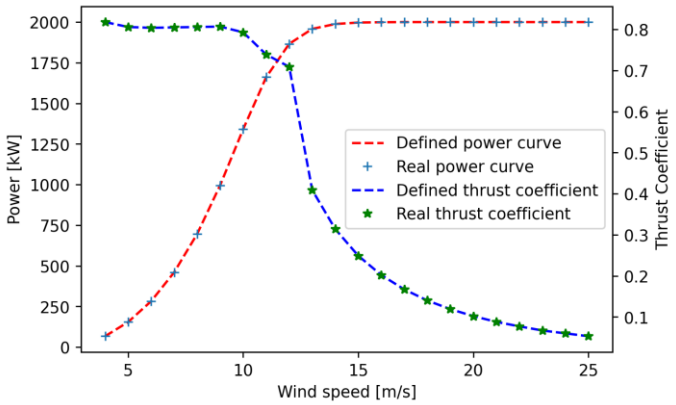

Figure 5.1: Simulated and real Power curve and thrust coefficient using Pywake.

As seen in Figure 5.1, the simulated results perfectly match the real data, to confirm this, a Python code was utilized to compute the percentage error for both the power curve and thrust coefficients, and the outcome indicated that both curves had no error, with a 0% value for each. This demonstrates the reliability and accuracy of the Pywake simulator in calculating the thrust coefficients and power of any wind turbine that is already implemented in its WindTurbines objects.

5.2 Total AEP of Horns Rev 1

The Annual Energy Production is an estimate of the amount of electricity that a wind farm is expected to generate over the course of a year. This estimate takes into account several factors such as wind conditions, turbine performance, and downtime for maintenance. Therefore, the actual energy output of a wind farm may differ from the estimated one. The AEP is an important characteristic of a wind farm, as it helps wind energy developers to determine the potential output of the farm and to plan its capacity and profitability.

Based on the information found on the website of the Danish Energy Agency [55], the average annual energy production of Horns Rev 1 in 2022 amounted to 566.982 GWh, where it is ideally around 600 GWh [56], thus it will be used as reference. In section 4.1, it was noted that Pywake can be used to simulate the total annual energy production of Horns Rev 1 as well as any other implemented wind farm. Thus, Figure 5.2(a) displays the correlation between the AEP and wind speed, while Figure 5.2(b) exhibits the relationship between the AEP and wind direction. In this simulation, default parameters were utilized due to the unavailability of actual data on the annual energy production of Horns Rev 1.

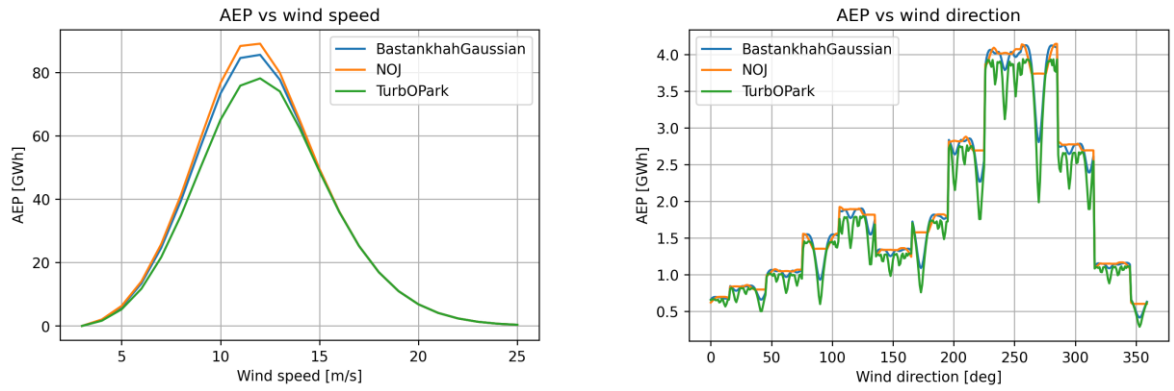

(a) (b)

Figure 5.2: The Annual energy production of horns rev 1 against wind speed (a), as well as against wind direction (b) using three wake models.

The confidential nature of the data required certain agreements that could not be made within the given time frame. Therefore, the AEP was plotted as a means of comparing the performance of different models in estimating it. The results, as illustrated in Figure 5.2, demonstrate that the NOJ model yielded the highest estimate of the AEP, while the TurbOPark model generated the lowest. The Bastankhah model's estimates were positioned between those of the other models.

In addition, Table 5.1 presents the results of the AEP simulation, which is the integrated values of the curves, using the three different models.

Table 5.1: Simulated AEP of Horns Rev 1 using three wake models.

Real AEP = 566.982 GWh			
Wake Model	**BastankhahGaussian**	**NOJ**	**TurbOPark**
Total AEP (GWh)	682.040725	702.435158	634.458807

Based on the results seen in Figure 5.2 and Table 5.1, the three wake models overestimated the actual annual energy production, with the closest result being from the TurbOPark model at 634.46 GWh.

It should be emphasized that simulation outcomes are frequently employed as approximations or forecasts and may not invariably align with real-world outcomes. The variability of wind conditions from year to year, which affects the wakes within the farm and ultimately influences

the annual energy production, could be the primary cause for the minor discrepancies observed between the simulated and actual data impacting the power output of wind farms.

5.3 First data case

The initial dataset corresponds to the simulation that utilized the data collected by Pena et al. [43] as a reference for simulating on row 7, as shown in Figure 5.3, with a wind direction of 270˚, which corresponds to the wind direction that is parallel to row 7 of the farm, in addition to wind directions of 221˚ and 132˚ with their corresponding turbine rows shown in Figure 5.6 and Figure *5.8* respectively. As a result, different scenarios are associated with different widths of wind direction in the simulations.

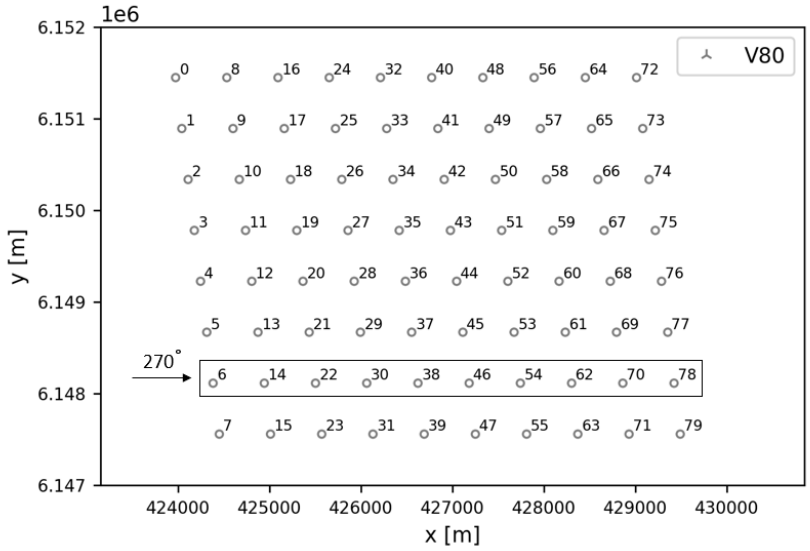

Figure 5.3: Schematics of the Horns Rev 1 farm turbines the those of row 7 for the wind direction 270˚.

Turbines 6, 14, 22, 30, 38, 46, 54, 62, 70, and 78 form row 7, and thus the power of each turbine is simulated and compared to its reference value collected, and the results are displayed as the power deficit versus the wind turbine number.

As a definition, power deficit refers to the difference between the ideal power that a wind turbine should produce under normal operating conditions, and the actual power output that it generates due to various factors such as turbulence, wake effects, and other environmental or technical limitations. It is a measure of the lost energy potential and can have a significant impact on the overall performance and efficiency of wind farms. Therefore, the less the power deficit, the better efficiency.

The outcomes of the simulation and SCADA analysis by Pena et al.[43] are expressed by taking the power deficit as:

$$Power\ Deficit = 1 - \frac{P_i}{P_j} \tag{6.1}$$

Here, P_i represents the power of the turbine i that is downstream the first turbine of the row, which is experiencing the free stream wind and has power value of P_j.

When the wind blows from directions 270˚ and 221˚, turbine 6 is considered the reference turbine because it receives a smooth and uninterrupted flow of wind without any turbulence from the wake of other turbines. On the other hand, when the wind comes from direction 132˚, turbine 78 becomes the reference turbine.

Figure 5.4 below illustrates the results of estimating the probability of wind speed from any direction, including the ones being used, using Pywake at Horns Rev 1.

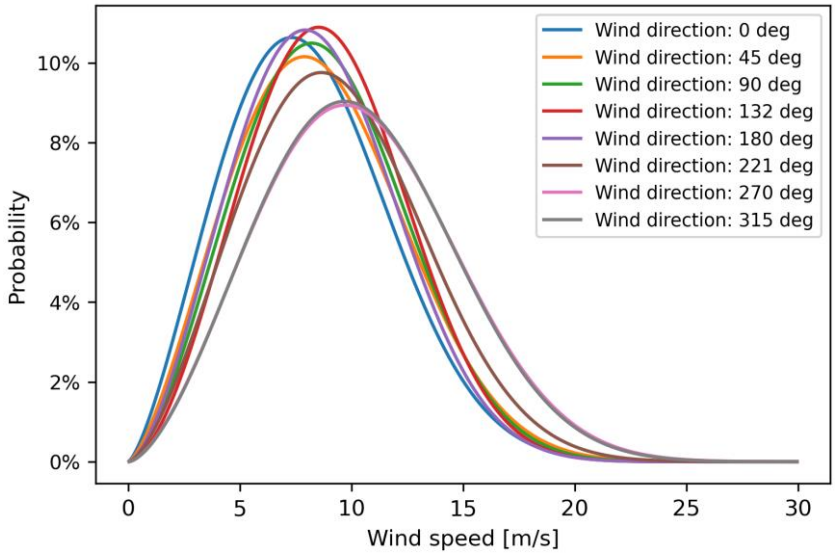

Figure 5.4: Wind speed distribution at Horns Rev 1

According to Figure 5.4, the wind speed with the highest probability is approximately 8-10m/s. For instance, when the wind is blowing from direction 221˚, there is a peak probability of almost 10% for wind speeds between 8-9 m/s at that direction.

Nevertheless, It is important to note that the estimated probabilities presented here are subject to variation in real-life scenarios, as wind speeds are heavily influenced by factors such as seasonal changes and weather conditions. Consequently, these findings serve as a useful guide and provide a general understanding of wind speeds, rather than providing precise predictions.

5.3.1 Wind direction 270˚

The power deficit for the wind turbines in row 7 under wind direction 270˚ is simulated using the three models, and the results are presented in Figure 5.5. The black dots on the curve represent the data extracted from the figures of Pena et al.[43] for Horns Rev 1, whereas the other curves represent the results from each wake model.

The case of wind direction 270˚ with width +/- 2.5˚ was not presented as its results were similar to the case of +/- 0˚, since the difference is considered to be very small.

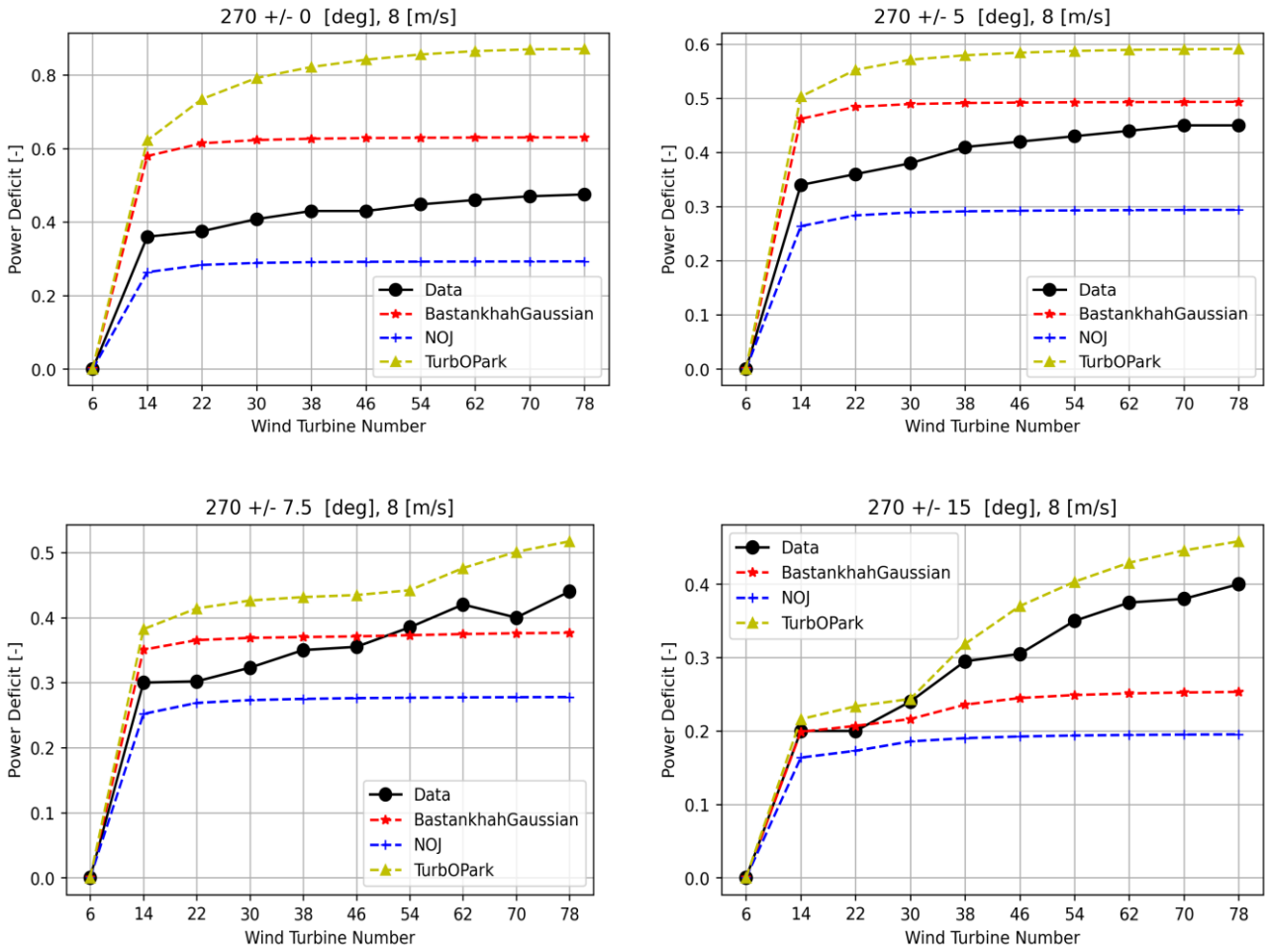

Figure 5.5: Power deficit in row 7 results using four different widths at wind direction 270˚.

The estimated power deficit for the turbines of row 7, as shown in Figure 5.5, is higher at narrow wind directions and decreases as the width of the wind direction interval increases. For instance, at wind direction 270 +/- 2.5˚, the estimated power deficit by TurbOPark model of turbine 14 is around 0.6, while at direction 270 +/-15˚, it decreased to 0.21. Moreover, it is noticable from the above graphs that the errors between the real data and the simulated results

decrease as the directional width increases. This could be attributed to the fact that with wider directional intervals, the upstream wakes of the turbines are less likely to directly impact the downstream turbines, resulting in less power loss. Therefore, when considering a very narrow range of wind directions for a wind turbine, the effect of wind direction uncertainty becomes more significant, and thus the turbines will be more sensitive to any variations in the wind direction. In other words, small changes in the wind direction can have a substantial impact on the turbine's performance, resulting in an increased level of uncertainty. Wind direction uncertainty may arise not only from the small natural variations but also from the yaw misalignment between turbines and wind, however, in this work it is not taken into consideration.

The simulation results of the three models closely resembled the real data, but each model had its own strengths and weaknesses. Specifically, the TurbOPark wake model tended to overestimate the power deficit in all directional bands, while the NOJ model consistently underestimated the power deficit values for the wind turbines in row 7 across all directions. On the other hand, the BastankhahGaussian model tended to overestimate the real data for directional widths of +/- 2.5˚ and +/- 5˚ as well as for turbines 14, 22, 30, 38, and 46 in the case of +/- 7.5˚ width. However, it then underestimated the power deficit values for the downwind turbines. For the +/- 15˚ direction band, the BastankhahGaussian model accurately estimated the power deficit of the second and third turbines of row 7 (14 and 22) but underestimated the power deficit values for the remaining turbines in the row.
Furthermore, an interesting observation is that as the directional band widens, the difference between the real data and the simulated data produced by the TurbOPark model becomes smaller and eventually becomes almost negligible, indicating a higher level of accuracy in the model's results.

In summary, while each model produced simulation results that were similar to the real data, they also had their own specific tendencies and limitations.

5.3.2 Wind direction 221 +/- 5˚

When wind is blowing from the 221˚ direction, the row of turbines facing this direction changes from row 7 to the diagonal row comprising turbines 6, 13, 20, 27, 34, 41, and 48, as illustrated in Figure 5.6. The spacing between the turbines in this newly facing row is greater compared to the turbines in row 7. Specifically, while the inter-turbine distance in row 7 is approximately

560 m, equivalent to roughly 7 turbine rotor diameters, the inter-turbine distance in the new row is approximately 750 m, which corresponds to around 9.4 rotor diameters.

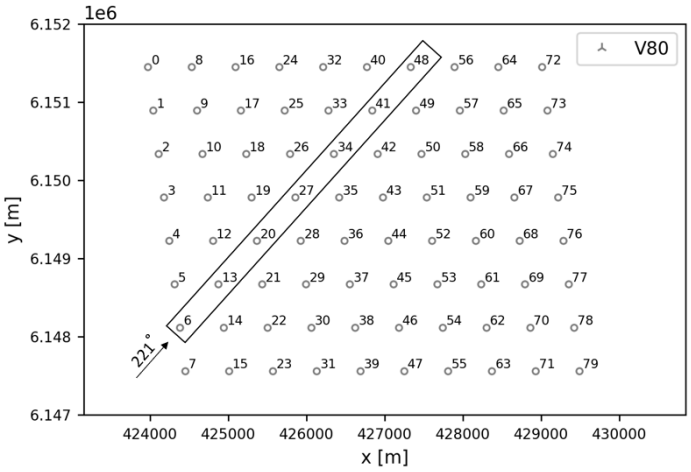

Figure 5.6: Turbine row that faces the wind direction of 221˚.

The power deficit for the turbines mentioned earlier has been also simulated using Pywake with the aid of the three models. The results are depicted in Figure 5.7.

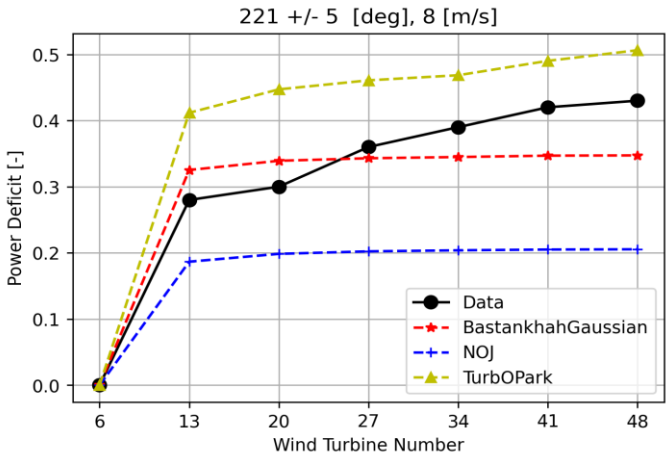

Figure 5.7: Power deficit versus at the row that faces the wind direction 221 +/- 5˚

In comparison to the simulations of the case with wind direction of 270 +/- 5˚, the simulations of the current scenario exhibit similar behavior. However, the power deficits are lower, and this might be due to the greater spacing between turbines, which results in downstream turbines being subjected to lesser wake effects from the upstream turbines. This observation is consistent with the general understanding that increased spacing between wind turbines is conducive to minimizing wake losses and increasing overall energy production efficiency.

Furthermore, the results indicate that the Bastankhah-Gaussian model closely approximates the power deficit for the second, third, fourth, and fifth turbines in the row, with numbers 13, 20,27 and 34 respectively, whereas the TurbOPark model provides the closest results for the last two turbines, 41 and 48, however, it overestimated all the real data. Conversely, the NOJ model exhibits a comparatively large estimation error in predicting the power deficit for the turbines, as it substantially underestimates the values.

5.3.3 Wind direction 132 +/- 5˚

Figure 5.8 illustrates the row of turbines that face the wind direction of 132˚. Presently, the wind is blowing from the south-east direction towards the wind farm. This row comprises turbines 78, 69, 60, 51, 42, 33, and 24, where the wind first hits turbine 78.

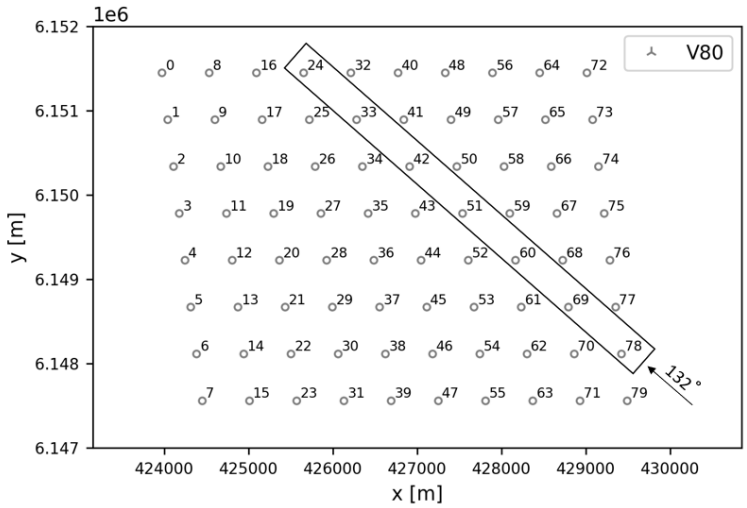

Figure 5.8: Turbine row that faces the wind direction of 132˚.

The inter-turbine distance in the present row is greater than that of the two previously mentioned rows, measuring around 10.4 turbine diameters which is approximately 0.83 km. This greater distance between turbines is expected to result in a reduced power deficit for this row.

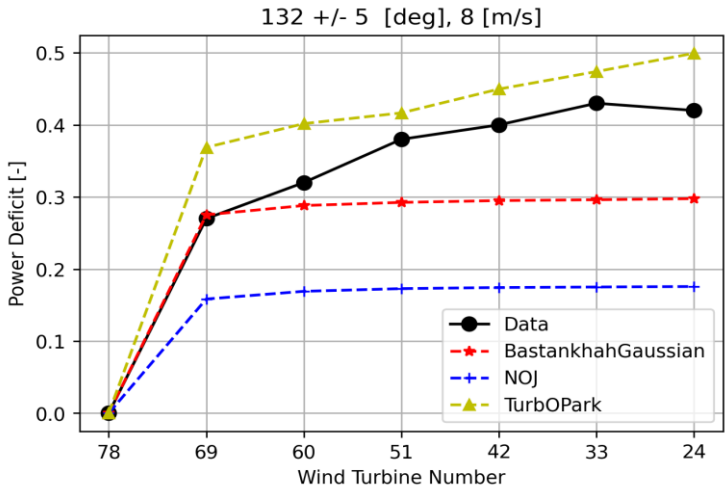

Figure 5.9: Power deficit versus at the row that faces the wind direction 132 +/- 5˚

Figure 5.9 illustrates the simulation results of the three wake models on the row facing the wind direction of 132˚. The BastankhahGaussian model accurately predicted the power deficit of the second turbine in the row, turbine number 69, and closely estimated the power deficit of the third turbine, turbine number 60, and underestimated the power deficit of the downstream turbines in the row. However, the TurbOPark model yielded results closest to the actual data for the fourth, fifth, sixth, and seventh turbines, although it is still overestimating the power deficit. The reason for this could be linked to the assumption made by the TurbOPark model that the wake expands as it moves downstream from the turbine. Furthermore, the model takes into account the level of atmospheric turbulence and assumes that the growth of the wake is a function of the turbulence intensity. As the distance downstream from the turbine increases (10.4 turbine diameters in this case), the turbulence intensity approaches the ambient turbulence intensity, which may explain the difference in predictions. Conversely, the NOJ model continues to underestimate the actual data significantly, providing no new insight into its effectiveness in predicting power deficits.

5.3.4 Power deficit of Horns Rev 1

Using the wake models available in Pywake, it is possible to compute and visualize the power deficit of the entire wind farm as a function of wind direction at any wind speed, as demonstrated in Figure 5.10 where a wind speed of 8 m/s is utilized.

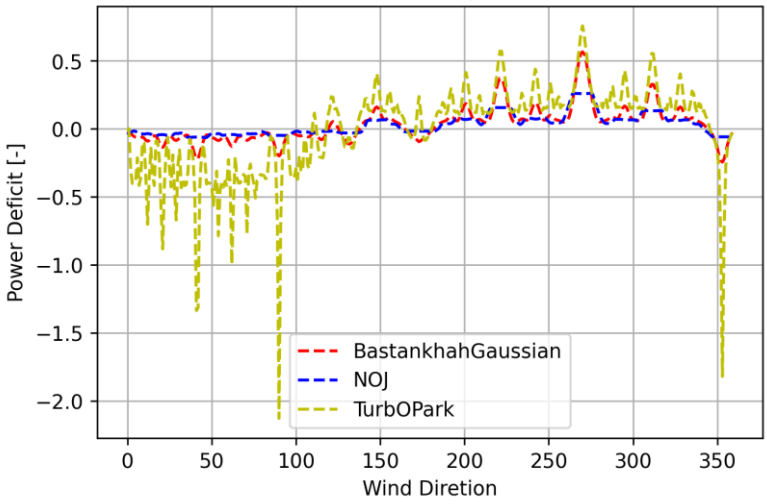

Figure 5.10: Power deficit of Horns Rev 1 against all wind directions at 8 m/s wind speed.

However, due to data constraints, only the real data for wind directions within the range of 250˚ to 290˚ can be obtained from Pena et al. [43]. Therefore, Figure 5.11 illustrates the power deficit for these specific wind directions, calculated using the three wake models.

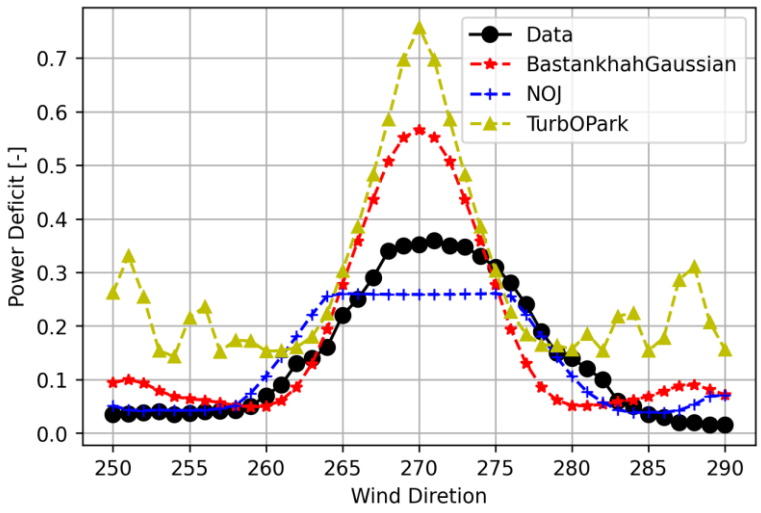

Figure 5.11: Power deficit of Horns Rev 1 as a function at wind directions relative to 270˚ at wind speed 8 m/s.

Although the wake models implemented in Pywake resulted in similar patterns to the actual data, each model produced distinct values. The NOJ model had the closest approximation to

the real data, but it indicated a constant power deficit value of around 0.259 for wind directions between 265˚ to 275˚, which was less than the value of the real data. Conversely, the TurbOPark model overestimated the real data in almost all directions except from 275˚ to 280˚, and showed fluctuations in the power deficit between directions 250˚ to 260˚ and 280˚ to 290˚. This fluctuation could be attributed to TurbOPark considering atmospheric turbulence intensity and other weather variables. Finally, the BastankhahGaussian model overestimated the real data in some directions and underestimated it in others.

5.4 Second data case

The average normalized power as a function of wind turbine number in row 7 for a free-stream wind speed of 8 m/s for seven wind directions, from 255˚ to 285˚ with an interval of 5˚ as derived from the three wake models and observations are shown in Figure 5.12. The reference data for this case are collected the figure in the work of Barthelmie et al. [42], as they used different models to simulate the normalized power of turbines of row 7 in Horns Rev 1.

As a definition, the normalized power of a wind turbine refers to the ratio of the actual power output of the turbine to the maximum power output that it could theoretically produce at its rated wind speed. This normalized power is used to assess the performance of the turbine under different wind conditions. By normalizing the power output in this way, it is possible to compare the performance of different wind turbines in a wind faram and evaluate their efficiency over time, accounting for changes in wind speed and other factors that may affect their output. In this study, the power output of each turbine located in row 7 is normalized to that of turbine number 6. The reason for this normalization is that all turbines in the row are of the same type, and turbine number 6 is assumed to be operating normally as it is experiencing unwaked wind flow.

There is good agreement between models and measurements in most wind directions in Figure 5.12, except at 255˚ and 260˚ where the observed values appear to be lower than the simulated results by the models.

When the wind direction was at 255˚, the TurbOPark model correctly predicted the power output of turbine number 38. However, the model overestimated the power output of the other turbines in the row. Despite this, the predictions of the TurbOPark model were the closest to the actual data compared to the other models tested. Interestingly, all three models gave the same power output for the first three turbines in the row at this direction. After the third turbine, however, the models provided different predictions. This discrepancy might be due to the fact that the models assume the first three turbines are unaffected by wake effects, whereas the other turbines are impacted by wakes generated by the turbines upstream in the wind farm. NOJ model gave the least wake loss followed by the BastankhahGaussian model and then the TurbOPark model.

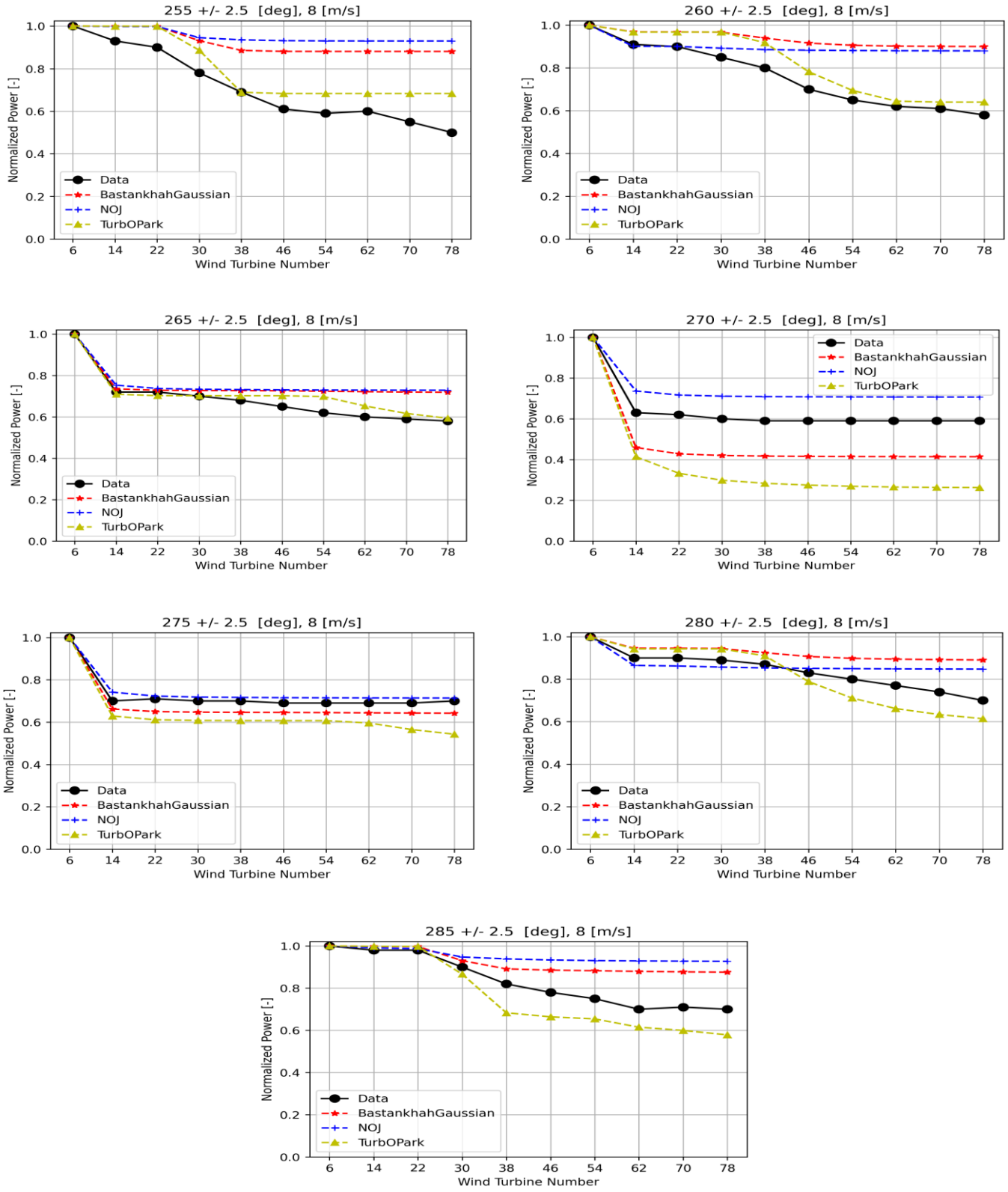

Figure 5.12: Normalized Power of each wind turbine of row 7 at different wind directions using the second data set.

For wind direction 260˚, both the TurbOPark and BastankhahGaussian models produced identical normalized power output results for the first four turbines, but diverged in their predictions for the remaining turbines while overestimating the actual data. Despite this, the TurbOPark model's results were closest to the actual data from the sixth turbine (number 46) to the last turbine (number 78). In contrast, the NOJ model gave the same results for the first three turbines, but overestimated the remaining turbines with a constant value. This disparity may be due to the fact that the NOJ model's velocity deficit is only affected by the downstream distance of the turbine.

The models exhibited a similar trend at wind direction 265˚ as they did at 260˚, but with less deviation between the observed and simulated data. All three models provided almost accurate power predictions for the first four turbines, but began to deviate from the actual data beyond the fourth turbine. The NOJ and BastankhahGaussian models produced similar results, both overestimating the power output for the entire row of turbines. The TurbOPark model also overestimated the power output for sixth, seventh and eighth turbines (46, 54, and 62), but was able to more accurately predict the power output for the last two turbines (70 and 78).

For wind directions 270˚ and 275˚, all three models demonstrated similar trends, with the NOJ model overestimating the actual values and both the BastankhahGaussian and TurbOPark models underestimating them. However, for both directions, the NOJ model provided the closest results compared to the real data. The errors were more significant for 270˚ than for 275˚, likely due to the fact that when the wind comes from 270˚, it is parallel to row 7, resulting in greater wake directly affecting the downstream turbines.

At direction 280˚, the TurbOPark and the BastankhahGaussian models produced similar power results for the initial five turbines while overestimating the collected farm data. BastankhahGaussian model continued to over predict the power for the last five turbines, at the time TurbOPark underestimated it. Nonetheless, TurbOPark provided the closest results to the actual data. The power of the second third and fourth generators calculated by the NOJ model were less than the actual power, while the power of the fifth and sixth turbines (38 and 46) was correctly predicted by the model, and then the model provided higher power values than the real values for the last four turbines.

At the last wind direction used, which is 285˚, the models predicted the power for the first three turbines correctly and then the NOJ and BastankhahGaussian models overestimated the power

where TurbOPark underestimated it. This is since the wake losses after the third turbine are unpredictable.

Overall, the performance of TubOPark model looked promising in most of the directions as it provided similar results for the normalized power of the turbines, except at direction 270˚. The NOJ model over predicted the results in most of the cases except at direction 280˚ for the first four turbines. BastankahGaussian also overestimated the data, except for directions 270˚ and 275˚. Moreover, the values of the normalized power were high compared to direction 270˚. This is because, in directions other than 270˚ (at which wind flows parralel to row 7), the turbines in row 7 are affected by wakes from turbines in other rows in the wind farm and may not be influenced by the wakes produced by the turbines of row 7. The small directional width taken into account (+/- 2.5˚) may also explain why the values of the normalized power for direction 270˚ are smaller compared to the values in other directions.

5.5 Wind farm flow map

Using various models, Pywake can visualize the flow map across a wind farm and illustrate the wake flow behind the turbines at different wind speeds and wind directions. It was fascinating to observe the flow maps of Horns Rev 1 through the different wake models. In Figure 5.13(a), the flow map is illustrated using the NOJ model, while Figure 5.13(b) exhibits the flow map using the BastankhahGaussian model.

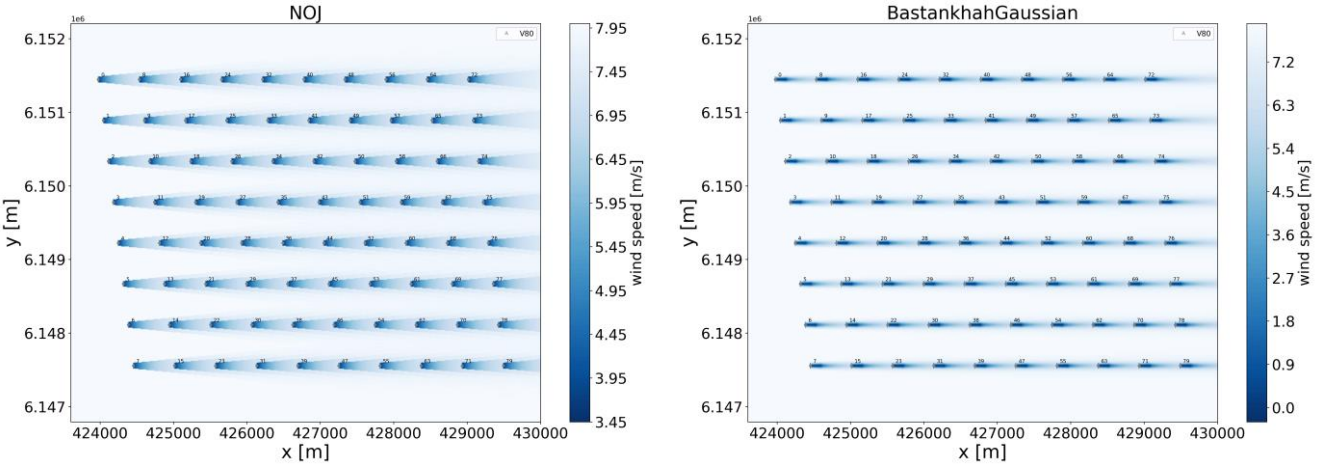

(a) (b)

Figure 5.13: Wake flow map for Horns Rev 1 wind farm using NOJ (a) and BastankhahGaussian (b) wake models.

In Figure 5.13(a), the NOJ model portrays the wake behind the turbines as expanding linearly as distance increase. However, the shape and behavior of the wake behind the turbine produced by BastanlhahGaussian model in Figure 5.13(b) are visibly different from the wake pattern by NOJ due to the use of different wake models. The BastankhahGaussian model assumes that the wake shape follows a Gaussian distribution, which affects the expansion rate (which is a funtion of the turbulence intensity) and behavior of the wake compared to the NOJ model that assumes the wake expands linearly with distance downstream the wind turbine. As a result, the flow map generated using the BastankhahGaussian model has a unique wake pattern that is distinguishable from the linear wake pattern seen in the NOJ model.

It would have been informative and interesting to observe how TurbOPark represents the wake distribution behind the wind turbines in the farm and compare it to the other models. Regrettably, a coding error prevented this analysis from being conducted within the allocated time. Additionally, since the flow maps were generated and incorporated at the end of the project, there was no opportunity to address the coding issue and assess the TurbOPark wake distribution.

6 Conclusion

In this thesis, the primary objective was to investigate the accuracy and sensitivity of three wake models, namely NOJ, BastankhahGaussian, and TurbOPark, implemented in the Pywake tool using real data from an offshore wind farm in the North Sea along the coast of Denmark, specifically Horns Rev 1. The models were used to simulate the Annual Energy Production (AEP) of the wind farm, the power deficit, and the normalized power of turbines in row 7 at varying wind directions. The simulated results were then compared with real data collected from two previous studies on Horns Rev 1.

The findings revealed that all three models demonstrated some degree of inaccuracy in estimating the real data, which was expected due to the difficulty in predicting weather conditions and wind speeds at the farm's location and since default models paramteres where used that might differ from the real ones, such as wind speeds. However, TurbOPark showed the closest results to the real data where it predicted the trend in the variation of power while over predicting its amplitude. The NOJ model was effective in estimating the power deficit of the entire wind farm for wind directions between 250˚ and 290˚. In contrast, the models showed a close agreement to the collected real data in the case of normalized power of row 7 turbines.

However, it should be noted that discrepancies between the simulated and real data may be due to errors in collecting the data manually from the curves of the previous works oh Pena et al [33] and Barthelmie et al. [32], or models not considering wakes from other turbines in the farm in some cases. Furthermore, practical factors that migh occur physically in the wind farm, such as icing on the blades of wind turbines and torque affecting the rotor can cause delays in power production, which were not accounted for in the simulations. Moreover, engineering wake models used to estimate the production of offshore wind farms usually assume inflow homogeneity over the whole domain. Wind direction and speed uncertainties could also contribute to errors between the simulated and observed data, highlighting the importance of considering wind direction uncertainty when evaluating wind turbine performance.

In conclusion, the three wake models in Pywake performed satisfactorily in simulating the power of turbines in Horns Rev 1 while accounting for the wake effect. Further research is required to ensure that the models are properly calibrated and include the relevant physics, as in this study, default parameters of the models where used for the simulation. Although

engineering models of wind turbine interaction remain essential tools in energy yield calculations, improvements to these models are possible and additional validation with real data is necessary.

References

[1] "Summary of Natural Gas & Renewable Power Generation.pdf." Accessed: Jan. 19, 2023. [Online]. Available: https://cdn.theforage.com/vinternships/companyassets/ay2tsYxaTif7Nt6z7/AA4Bnq2tJHALwE8cg/1630539940015/Summary%20of%20Natural%20Gas%20&%20Renewable%20Power%20Generation.pdf

[2] "Wind Electricity – Analysis," *IEA*. https://www.iea.org/reports/wind-electricity (accessed Jan. 25, 2023).

[3] R. Valotta Rodrigues, M. Friis-Møller, K. Dykes, N. Pollini, and M. Jensen, "A surrogate model of offshore wind farm annual energy production to support financial evaluation," *J. Phys. Conf. Ser.*, vol. 2265, no. 2, p. 022003, May 2022, doi: 10.1088/1742-6596/2265/2/022003.

[4] N. Sedaghatizadeh, M. Arjomandi, R. Kelso, B. Cazzolato, and M. H. Ghayesh, "Modelling of wind turbine wake using large eddy simulation," *Renew. Energy*, vol. 115, pp. 1166–1176, Jan. 2018, doi: 10.1016/j.renene.2017.09.017.

[5] F. González-Longatt, P. Wall, and V. Terzija, "Wake effect in wind farm performance: Steady-state and dynamic behavior," *Renew. Energy*, vol. 39, no. 1, pp. 329–338, Mar. 2012, doi: 10.1016/j.renene.2011.08.053.

[6] P. Duffy, "Effect of wind speed gradients on AEP in a wind farm cluster," 2019, Accessed: Jan. 23, 2023. [Online]. Available: https://repository.tudelft.nl/islandora/object/uuid%3Ae0e318de-79e0-481c-82d3-4153e6cd9998

[7] J.-O. Mo, A. Choudhry, M. Arjomandi, R. Kelso, and Y.-H. Lee, "Effects of wind speed changes on wake instability of a wind turbine in a virtual wind tunnel using large eddy simulation," *J. Wind Eng. Ind. Aerodyn.*, vol. 117, pp. 38–56, Jun. 2013, doi: 10.1016/j.jweia.2013.03.007.

[8] D. Vahidi and F. Porté-Agel, "A New Streamwise Scaling for Wind Turbine Wake Modeling in the Atmospheric Boundary Layer," *Energies*, vol. 15, no. 24, Art. no. 24, Jan. 2022, doi: 10.3390/en15249477.

[9] R. J. Barthelmie, S. T. Frandsen, M. N. Nielsen, S. C. Pryor, P.-E. Rethore, and H. E. Jørgensen, "Modelling and measurements of power losses and turbulence intensity in wind turbine wakes at Middelgrunden offshore wind farm," *Wind Energy*, vol. 10, no. 6, pp. 517–528, 2007, doi: 10.1002/we.238.

[10] R. J. Barthelmie and L. E. Jensen, "Evaluation of wind farm efficiency and wind turbine wakes at the Nysted offshore wind farm," *Wind Energy*, vol. 13, no. 6, pp. 573–586, 2010, doi: 10.1002/we.408.

[11] M. De-Prada-Gil, C. G. Alías, O. Gomis-Bellmunt, and A. Sumper, "Maximum wind power plant generation by reducing the wake effect," *Energy Convers. Manag.*, vol. 101, pp. 73–84, Sep. 2015, doi: 10.1016/j.enconman.2015.05.035.

[12] J. K. Lundquist, K. K. DuVivier, D. Kaffine, and J. M. Tomaszewski, "Costs and consequences of wind turbine wake effects arising from uncoordinated wind energy

development," *Nat. Energy*, vol. 4, no. 1, Art. no. 1, Jan. 2019, doi: 10.1038/s41560-018-0281-2.

[13] Q. Li, T. Maeda, Y. Kamada, and Y. Hiromori, "Investigation of wake characteristic of a 30 kW rated power Horizontal Axis Wind Turbine with wake model and field measurement," *Appl. Energy*, vol. 225, pp. 1190–1204, Sep. 2018, doi: 10.1016/j.apenergy.2018.05.022.

[14] N. Charhouni, A. Arbaoui, and M. Sallaou, "Qualification of three analytical wake models," 2015.

[15] H. Sun and H. Yang, "Study on three wake models' effect on wind energy estimation in Hong Kong," *Energy Procedia*, vol. 145, pp. 271–276, Jul. 2018, doi: 10.1016/j.egypro.2018.04.050.

[16] T. Göçmen, M. P. van der Laan, P.-E. Réthoré, A. Diaz, G. Larsen, and S. Ott, "Wind turbine wake models developed at the technical university of Denmark: A review," *Renew. Sustain. Energy Rev.*, vol. 60, pp. 752–769, Jul. 2016, doi: 10.1016/j.rser.2016.01.113.

[17] R. Shakoor, M. Y. Hassan, A. Raheem, and Y.-K. Wu, "Wake effect modeling: A review of wind farm layout optimization using Jensen's model," *Renew. Sustain. Energy Rev.*, vol. 58, pp. 1048–1059, May 2016, doi: 10.1016/j.rser.2015.12.229.

[18] N. Sedaghatizadeh, M. Arjomandi, R. Kelso, B. Cazzolato, and M. H. Ghayesh, "Modelling of wind turbine wake using large eddy simulation," *Renew. Energy*, vol. 115, pp. 1166–1176, Jan. 2018, doi: 10.1016/j.renene.2017.09.017.

[19] J. Fischereit, K. Schaldemose Hansen, X. G. Larsén, M. P. van der Laan, P.-E. Réthoré, and J. P. Murcia Leon, "Comparing and validating intra-farm and farm-to-farm wakes across different mesoscale and high-resolution wake models," *Wind Energy Sci.*, vol. 7, no. 3, pp. 1069–1091, May 2022, doi: 10.5194/wes-7-1069-2022.

[20] R. Riva *et al.*, "Wind farm layout optimization with load constraints using surrogate modelling," *J. Phys. Conf. Ser.*, vol. 1618, no. 4, p. 042035, Sep. 2020, doi: 10.1088/1742-6596/1618/4/042035.

[21] I. G. W. Krabben, M. P. van der Laan, M. Koivisto, T. J. Larsen, M. M. Pedersen, and K. S. Hansen, "Why curved wind turbine rows are better than straight ones," *J. Phys. Conf. Ser.*, vol. 1256, no. 1, p. 012028, Jul. 2019, doi: 10.1088/1742-6596/1256/1/012028.

[22] M. P. van der Laan, S. J. Andersen, and P.-E. Réthoré, "Brief communication: Wind speed independent actuator disk control for faster AEP calculations of wind farms using CFD," Aerodynamics and hydrodynamics, preprint, May 2019. doi: 10.5194/wes-2019-27.

[23] "Power plants: Horns Rev 1 - Vattenfall." https://powerplants.vattenfall.com/horns-rev/ (accessed Jan. 25, 2023).

[24] "b. horns rev data.pdf." Accessed: Jan. 26, 2023. [Online]. Available: https://www.loveyassvalley.com/resources/b.%20horns%20rev%20data.pdf

[25] "Our offshore wind farms." https://orsted.com/en/our-business/offshore-wind/our-offshore-wind-farms (accessed Jan. 25, 2023).

[26] C. B. Hasager, N. G. Nygaard, P. J. H. Volker, I. Karagali, S. J. Andersen, and J. Badger, “Wind Farm Wake: The 2016 Horns Rev Photo Case,” *Energies*, vol. 10, no. 3, Art. no. 3, Mar. 2017, doi: 10.3390/en10030317.

[27] “Figure 2. Horns Rev 1 wind farm layout and met mast locations.,” *ResearchGate*. https://www.researchgate.net/figure/Horns-Rev-1-wind-farm-layout-and-met-mast-locations_fig2_333239218 (accessed Jan. 26, 2023).

[28] “Lillgrund Offshore Wind Farm - Renewable Technology.” https://www.renewable-technology.com/projects/lillgrund-offshore-wind-farm/ (accessed Apr. 12, 2023).

[29] A. Creech, W.-G. Früh, and A. Maguire, “Simulations of an Offshore Wind Farm Using Large-Eddy Simulation and a Torque-Controlled Actuator Disc Model,” *Surv. Geophys.*, vol. 36, Oct. 2014, doi: 10.1007/s10712-015-9313-7.

[30] “Problems with Wind Power.” https://www.basinandrangewatch.org/Wind-Searchlight-CloserLook.html (accessed Apr. 12, 2023).

[31] “979747.pdf.” Accessed: Apr. 12, 2023. [Online]. Available: https://www.osti.gov/etdeweb/servlets/purl/979747

[32] T. Göçmen and G. Giebel, “Estimation of turbulence intensity using rotor effective wind speed in Lillgrund and Horns Rev-I offshore wind farms,” *Renew. Energy*, vol. 99, Jul. 2016, doi: 10.1016/j.renene.2016.07.038.

[33] “Final report on the effect of Nysted Offshore Wind Farm on harbour porpoises”.

[34] “Extending the Nysted Wind Farm operational lifespan to 30+ years.” https://www.cotes.com/blog/extending-the-operational-lifespan-of-orsted-nysted-wind-farm (accessed Apr. 13, 2023).

[35] “Hard-working offshore wind farm turns ten.” https://orsted.com/en/media/newsroom/news/2013/12/hard-working-offshore-wind-farm-turns-ten (accessed Apr. 13, 2023).

[36] “Hywind Scotland.” https://www.equinor.com/energy/hywind-scotland (accessed Apr. 17, 2023).

[37] F. G. Nielsen, “Hywind – From idea to world’s first wind farm based upon floaters”.

[38] allsustainablesolutions, “Hywind Scotland | The First Floating Offshore Wind Farm in the World,” *All Sustainable Solutions*, Dec. 10, 2019. https://allsustainablesolutions.com/hywind-scotland-the-first-floating-offshore-wind-farm-in-the-world/ (accessed Apr. 17, 2023).

[39] A. Jacobsen and M. Godvik, “Influence of wakes and atmospheric stability on the floater responses of the Hywind Scotland wind turbines,” *Wind Energy*, vol. 24, Feb. 2021, doi: 10.1002/we.2563.

[40] M. Bahamonde, J. Macías, C. Rodríguez González, S. Litrán, and M. Herrera, “Modeling of the Wind Potential in the Open Sea and Its Application to the Calculation of Energy,” *Energies*, vol. 15, p. 1157, Feb. 2022, doi: 10.3390/en15031157.

[41] “Siemens SWT-6.0-154 - Manufacturers and turbines - Online access - The Wind Power.” https://www.thewindpower.net/turbine_en_807_siemens_swt-6.0-154.php (accessed Apr. 18, 2023).

[42] R. Barthelmie *et al.*, “Quantifying the Impact of Wind Turbine Wakes on Power Output at Offshore Wind Farms,” *J. Atmospheric Ocean. Technol. - J ATMOS OCEAN TECHNOL*, vol. 27, pp. 1302–1317, Aug. 2010, doi: 10.1175/2010JTECHA1398.1.

[43] A. Pena, P.-E. Rethore, C. B. Hasager, and K. S. Hansen, “Results of wake simulations at the Horns Rev I and Lillgrund wind farms using the modified Park model”.

[44] “Welcome to PyWake — PyWake 2.4.0 documentation.” https://topfarm.pages.windenergy.dtu.dk/PyWake/ (accessed Jan. 26, 2023).

[45] R. V. Rodrigues, “Wind farm flow modeling and optimization in PyWake/TOPFARM,” 2022.

[46] “Near Wakes - an overview | ScienceDirect Topics.” https://www.sciencedirect.com/topics/earth-and-planetary-sciences/near-wakes (accessed Feb. 08, 2023).

[47] “Validation_of_wind_turbine_wake_models.pdf.” Accessed: Feb. 14, 2023. [Online]. Available: https://www.menzio.de/images/Download/Validation_of_wind_turbine_wake_models.pdf

[48] M. K. Vinnes, S. Gambuzza, B. Ganapathisubramani, and R. J. Hearst, “The far wake of porous disks and a model wind turbine: Similarities and differences assessed by hot-wire anemometry,” *J. Renew. Sustain. Energy*, vol. 14, no. 2, p. 023304, Mar. 2022, doi: 10.1063/5.0074218.

[49] “Sikkeland_2020.pdf.” Accessed: Feb. 08, 2023. [Online]. Available: https://nmbu.brage.unit.no/nmbu-xmlui/bitstream/handle/11250/2725555/Sikkeland_2020.pdf?sequence=2&isAllowed=y

[50] “A note on wind generator interaction”.

[51] N. G. Nygaard, S. T. Steen, L. Poulsen, and J. G. Pedersen, “Modelling cluster wakes and wind farm blockage,” *J. Phys. Conf. Ser.*, vol. 1618, no. 6, p. 062072, Sep. 2020, doi: 10.1088/1742-6596/1618/6/062072.

[52] “TurbOPark.” Ørsted R&D, Dec. 01, 2022. Accessed: Feb. 20, 2023. [Online]. Available: https://github.com/OrstedRD/TurbOPark/blob/dfd43f920f655127abc24de0548be90f256e3127/TurbOPark%20description.pdf

[53] M. Bastankhah and F. Porté-Agel, “A new analytical model for wind-turbine wakes,” *Renew. Energy*, vol. 70, pp. 116–123, Oct. 2014, doi: 10.1016/j.renene.2014.01.002.

[54] M. Krutova, M. B. Paskyabi, F. G. Nielsen, and J. Reuder, “Evaluation of Gaussian wake models under different atmospheric stability conditions: Comparison with large eddy simulation results,” *J. Phys. Conf. Ser.*, vol. 1669, no. 1, p. 012016, Oct. 2020, doi: 10.1088/1742-6596/1669/1/012016.

[55] “Data: Oversigt over energisektoren,” *Energistyrelsen*, Aug. 25, 2016. https://ens.dk/service/statistik-data-noegletal-og-kort/data-oversigt-over-energisektoren (accessed Apr. 27, 2023).

[56] “Horns Rev | Vattenfall’s Power Plants.” https://web.archive.org/web/20110113032120/http://powerplants.vattenfall.com/powerplant/horns-rev (accessed Apr. 27, 2023).

Appendices

Appendix A – Thesis Description

University of South-Eastern Norway

Faculty of Technology, Natural Sciences and Maritime Sciences, Campus Porsgrunn

FMH606 Master's Thesis

Title: Comparing wind farm production data to engineering wake model simulations

USN supervisor: Geir Elseth

External partner: Equinor Porsgrunn, with Atle Johnsen Gyllensteen as co-supervisor

Task description:

- Part 1: Literature study. Collect offshore wind farm production data from public sources and publications.
- Part 2: Choose dataset.
- Part 3: Run the py_wake simulator and compare simulated production to observed production. Different wake models should be tested for sensitivity; NO Jensen, Park, TurbOPark etc.

Student category: EET or PT

Is the task suitable for online students (not present at the campus)? Yes

Practical arrangements: None

Supervision:
As a general rule, the student is entitled to 15-20 hours of supervision. This includes necessary time for the supervisor to prepare for supervision meetings (reading material to be discussed, etc).

Signatures:

Supervisor (date and signature):

Student (write clearly in all capitalized letters):

Student (date and signature):